PHYSICAL REVIEW D **81,** 085044 (2010)

Collective modes and instabilities in anisotropically expanding ultrarelativistic plasmas

Anton Rebhan and Dominik Steineder

Institut für Theoretische Physik, Technische Universität Wien, Wiedner Hauptstrasse 8-10, A-1040 Vienna, Austria

(Received 20 January 2010; published 28 April 2010)

The time evolution of collective modes in an expanding ultrarelativistic and (effectively) Abelian plasma is studied in the hard-loop approximation semianalytically by means of integrodifferential equations. A previous treatment is generalized to arbitrary orientation of wave vectors with respect to the direction of anisotropy and thus to a fully 3 + 1 dimensional situation. Moreover, initial fluctuations are allowed in both gauge fields and currents, which is necessary in the case of (stable) longitudinal modes. For unstable (Weibel) modes, this generalization of initial conditions reduces drastically the lower bound on the delay in the onset of growth that was found previously by considering only collective gauge fields as seeds. This makes it appear much more likely that non-Abelian plasma instabilities seeded by small initial rapidity fluctuations could play an important role in the early stage of heavy-ion collisions at LHC energies.

DOI: 10.1103/PhysRevD.81.085044 PACS numbers: 11.15.Bt, 04.25.Nx, 11.10.Wx, 12.38.Mh

I. INTRODUCTION

Fits of hydrodynamical models to the experimental results at the Relativistic Heavy Ion Collider (RHIC) [1–3] are often interpreted as an indication of an extremely fast thermalization, or at least isotropization, of the quark-gluon plasma that is assumed to have formed with initial temperatures significantly above the deconfinement temperature. The inferred thermalization time of $\lesssim 1$ fm/c is so short that is hard to understand from a perturbative framework such as the (original) bottom-up thermalization scenario [4–6]. Together with the low inferred value for the specific shear viscosity, it seems to clearly favor strong-coupling approaches, in particular those based on gauge-gravity duality [7].

However, as pointed out first by Ref. [8], a weak-coupling approach has to take into account the inevitable presence of non-Abelian (chromo-Weibel) plasma instabilities [9–12], which produce nonperturbatively large gauge fields that may lead to important, qualitative modifications of bottom-up thermalization [13–17]. Plasma instabilities and associated turbulent phenomena may even be responsible for a strong reduction of the effective shear viscosity [18]. A complete scenario, even of just the early stages of the evolution, is still missing, but would clearly be needed to decide, first, whether the thermalization of the quark-gluon plasma at RHIC is indeed a strong-coupling phenomenon and, second, what to expect if the early stage of heavy-ion collisions at the higher energies at the Large Hadron Collider (LHC) is probing a regime where weak-coupling approaches based on (resummed) perturbative quantum chromodynamics (QCD) become relevant.

At sufficiently weak coupling, the collective dynamics of a non-Abelian plasma can be described to leading order by an effective field theory produced by integrating out the hard modes corresponding to real (as opposed to virtual) plasma constituents. For anisotropic plasmas, the resulting hard-loop effective theory [19] is a generalization of the well-studied hard-thermal-loop effective theory [20–22]. The corresponding effective field equations are nonlocal, but can be made local at the expense of introducing a continuous set of auxiliary fields [23] which arise naturally when solving gauge-covariant Boltzmann-Vlasov equations [24–27]. In the hard-loop approximation, these auxiliary fields depend on the velocity vector of the hard particles whose hard momentum scale is integrated out.

The instabilities in a stationary homogeneous plasma with momentum-space anisotropy have been studied in this approximation in [8,28–31] for the case of weak fields, where the dynamics is effectively Abelian. In the Abelian case, instabilities grow exponentially until they are large enough to modify the distribution of the hard particles, typically giving rise to fast isotropization. In the non-Abelian case, nonlinear self-interactions of the collective fields may hinder this evolution, which can only be studied by a numerical (real-time lattice) treatment. The first numerical simulations of non-Abelian plasma instabilities have only considered modes that are constant in the directions transverse to the direction of momentum anisotropy [32]. In this situation there is a short stagnation of the exponential growth when the non-Abelian regime is entered, after which localized Abelianization occurs together with continued exponential growth. However, in the more generic case of fully 3 + 1-dimensional evolution [33,34], such local Abelianization appears to get largely destroyed. Instead, a turbulent cascade [15,35] is formed where the growth is reduced to a linear one (see however [36,37]). This was also found in more extensive simulations with stronger anisotropies in [38], although only when initial fields were already nonperturbatively large.

In Ref. [39] the hard-loop effective theory for stationary anisotropic plasmas was extended to the case of a boost-invariant, longitudinally expanding distribution of plasma

particles, which is closer to the actual situation in the earliest stage of heavy-ion collisions. In the expanding case, more and more modes become unstable as the expansion increases the momentum anisotropy, while the growth rate of each unstable mode decreases with the density of the plasma. In [40] first numerical results for the non-Abelian evolution were obtained, albeit still restricted to the effectively 1 + 1-dimensional situation of modes that are constant in transverse directions. In this case, continued approximately exponential growth was observed (albeit only exponential in the square root of proper time due to the linearly decreasing density of the plasma).

In the expanding case, even the time evolution in the weak-field regime is nontrivial and cannot be given in closed form. However, in Ref. [39] integrodifferential equations were obtained which made it possible to study the time evolution semianalytically in the case of effectively 1 + 1-dimensional dynamics. As a preparation of fully 3 + 1-dimensional real-time lattice studies of non-Abelian plasma instabilities in expanding plasmas, we shall generalize the semianalytical treatment of Ref. [39] to arbitrary wave vectors of the collective modes.

At the same time, we shall generalize to arbitrary initial conditions, allowing for seeds both in the collective gauge fields (the case considered in [39,40]) and also in the auxiliary fields corresponding more directly to colored fluctuations in the hard particle distribution. While in the case of stationary anisotropic plasmas little difference was found between the two possibilities for introducing seed fields for instabilities, in the expanding case we find that this generalization reduces dramatically the uncomfortably long delay of the onset of growth that was observed in [39,40]. As will be discussed in more detail below, this in fact reverts some of the negative conclusions of Refs. [39,40] concerning the possible role of plasma instabilities in heavy-ion collisions for explaining very early thermalization. While at RHIC energies with parameters matched from color-glass-condensate scenarios [41], there is still somewhat too little room for plasma instabilities that grow from small initial rapidity fluctuations, the situation at LHC energies, which appeared somewhat marginal in Refs. [39,40], is now much more favorable with regard to an important role of such plasma instabilities if the quark-gluon plasma to be produced at the LHC is described by the weak-coupling physics underlying the hard-loop-resummed treatment.

II. HARD-LOOP EFFECTIVE FIELD EQUATIONS WITH ANISOTROPICALLY EXPANDING BACKGROUND

A (sufficiently small) gauge coupling g introduces a hierarchy of smaller momentum scales below the scale of "hard" momenta $|\mathbf{p}| = p^0$ of ultrarelativistic plasma constituents. The "soft" scale $\sim g\sqrt{f}|\mathbf{p}|$, where f is the typical hard particle occupation number, is associated with different screening phenomena and the various branches of plasmon propagation. To leading order they are described by hard (thermal) loop effective theories. When $f(\mathbf{p})$ is anisotropic, the soft scale is also the domain of plasma instabilities, which constitute the dominant nonequilibrium effects at weak coupling: the associated rates are parametrically larger than any of the scattering processes among plasma particles.

As long as the amplitude of the gauge fields $A \ll \sqrt{f}|\mathbf{p}|$, the evolution of the plasma instabilities is essentially Abelian and can be studied by a perturbative linear-response analysis. For a stationary anisotropic plasma, the evolution is simply exponential in time until non-Abelian self-interactions might hinder further growth when $A \gtrsim \sqrt{f}|\mathbf{p}|$ and thereby delay the isotropization coming from the backreaction of the collective fields on the distribution of hard plasma particles. In an expanding plasma, the Abelian (weak-field) regime is complicated by the counterplay of increasing anisotropy, which favors the appearance of plasma instabilities, and dilution of hard particle densities as well as energy densities in soft collective fields.

In the following we shall first recapitulate the hard-loop effective field equations for an anisotropically expanding non-Abelian plasma as introduced in Refs. [39,40], and later specialize to the effectively Abelian weak-field regime. In view of the numerical simulations that were carried out to study the non-Abelian, strong-field regime, the Abelian evolution can be expected to provide an upper limit on the strength of plasma instabilities that are seeded by small initial fluctuations.

A. Boost-invariant expanding background

We assume a color-neutral background distribution of plasma particles $f_0(\mathbf{p}, \mathbf{x}, t)$ which satisfies

$$v \cdot \partial f_0(\mathbf{p}, \mathbf{x}, t) = 0, \qquad v^\mu = p^\mu/p^0. \tag{2.1}$$

This is satisfied trivially in a stationary homogeneous plasma with arbitrary momentum anisotropy. In order to describe the earliest stage of heavy-ion collisions in the limit of large nuclei, we consider a plasma that expands in one spatial direction (the beam axis). Requiring boost invariance [42] and isotropy in the transverse directions, we are led to [43,44]

$$f_0(\mathbf{p}, x) = f_0(p_\perp, p^z, z, t) = f_0(p_\perp, p'^z, \tau), \tag{2.2}$$

where the transformed longitudinal momentum is

$$p'^z = \gamma(p^z - \beta p^0), \qquad \beta = z/t, \qquad \gamma = t/\tau, \qquad \tau = \sqrt{t^2 - z^2}, \tag{2.3}$$

with $p^0 = \sqrt{p_\perp^2 + (p^z)^2}$ for ultrarelativistic (massless) particles.

Introducing the comoving coordinates of proper time τ and space-time rapidity η through

$$\begin{aligned} t &= \tau\cosh\eta, \qquad \beta = \tanh\eta, \\ z &= \tau\sinh\eta, \qquad \gamma = \cosh\eta, \end{aligned} \tag{2.4}$$

we are led to a coordinate system with nontrivial metric

$$ds^2 = g_{\alpha\beta}dx^\alpha dx^\beta \equiv d\tau^2 - d\mathbf{x}_\perp^2 - \tau^2 d\eta^2, \tag{2.5}$$

where indices from the beginning of the Greek alphabet will be reserved for the new coordinates. Latin indices will from now on only refer to the two transverse spatial directions. Despite the nontrivial metric, we shall only use ordinary derivatives when writing for instance $D_\alpha = \partial_\alpha - ig[A_\alpha, \cdot]$ for gauge-covariant derivatives.

In addition to space-time rapidity η, we also introduce momentum-space rapidity y for the massless particles according to

$$p^\mu = p_\perp(\cosh y, \cos\phi, \sin\phi, \sinh y). \tag{2.6}$$

In comoving coordinates, we then have

$$\begin{aligned} p^\tau &= \sqrt{p_\perp^2 + \tau^2(p^\eta)^2} = p^0\cosh\eta - p^z\sinh\eta \\ &= p_\perp\cosh(y-\eta), \end{aligned} \tag{2.7}$$

$$\begin{aligned} p^\eta &= -p_\eta/\tau^2 = (p^z\cosh\eta - p^0\sinh\eta)/\tau \\ &= p'^z/\tau = [p_\perp\sinh(y-\eta)]/\tau. \end{aligned} \tag{2.8}$$

Equation (2.1), where the space-time derivatives act at fixed $\mathbf{p}_\perp$ and p^z, becomes

$$(p^\alpha\partial_\alpha)f_0|_{p^\mu} = 0 \tag{2.9}$$

with fixed p^μ and thus fixed $p_\perp$, y, ϕ as opposed to fixed p^α. This is solved by any function of the form $f_0(\mathbf{p}, \mathbf{x}, t) = f_0(\mathbf{p}_\perp, p_\eta)$, taking into account that p_η depends on τ and η according to (2.8). We choose

$$f_0(\mathbf{p}, x) = f_{\rm iso}\Big(\sqrt{p_\perp^2 + p_\eta^2/\tau_{\rm iso}^2}\Big) = f_{\rm iso}\Bigg(\sqrt{p_\perp^2 + \Big(\frac{p'^z\tau}{\tau_{\rm iso}}\Big)^2}\Bigg) \tag{2.10}$$

which corresponds to a locally isotropic distribution on the hypersurface $\tau = \tau_{\rm iso}$ with increasingly oblate momentum-space anisotropy at $\tau > \tau_{\rm iso}$ but prolate anisotropy for $\tau < \tau_{\rm iso}$.[1] We shall also have to consider a lowest value of proper time, τ_0, where a particle description of the plasma constituents begins to make sense. Depending on whether the parameter $\tau_{\rm iso}$ is smaller or larger than τ_0, we shall consider a plasma that starts with oblate or prolate momentum distribution.

[1]Notice that $\tau_{\rm iso}$ is just a parameter of the background distribution and does not refer to the time where isotropization of the plasma eventually occurs through interactions.

The particle distribution function (2.10) has the same form as the one used in Refs. [28,29,32,34], but the anisotropy parameter ξ introduced therein is now space-time dependent according to

$$\xi(\tau) = (\tau/\tau_{\rm iso})^2 - 1, \tag{2.11}$$

and the normalization factor $N(\xi)$ of Refs. [29,32,34] is unity. (The anisotropy parameter θ used in Ref. [17] is related to ξ by $\xi \sim \theta^{-2}$ for large anisotropies.) The behavior $\xi \sim \tau^2$ at large τ corresponds to having a free-streaming background distribution. In a more realistic collisional plasma, ξ will have to grow slower than this. In the first stage of the original bottom-up scenario [13], ignoring plasma instabilities, one would have had $\xi \sim \tau^{2/3}$. In Ref. [14] it was argued that plasma instabilities reduce the exponent to $\xi \sim \tau^{1/2}$, whereas Ref. [17] recently presented arguments in favor of $\xi \sim \tau^{1/4}$. All these scenarios typically consider $\xi \gg 1$, so below we shall mostly concentrate on the case $\tau_{\rm iso} < \tau_0$ and thus high anisotropy for all $\tau > \tau_0$, but in the simplified case of a collisionless free-streaming expansion. However, we shall also discuss instabilities in prolate phases for which we need to set $\tau_{\rm iso} > \tau_0$.

B. Hard-expanding-loop effective field equations

In an approximately collisionless plasma, the gauge-covariant Boltzmann-Vlasov equations for color charge carrying perturbations δf_a have the form

$$v\cdot D\delta f_a(\mathbf{p}, \mathbf{x}, t) = g v_\mu F_a^{\mu\nu}\partial_\nu^{(p)} f_0(\mathbf{p}, \mathbf{x}, t). \tag{2.12}$$

In comoving coordinates we write

$$V\cdot D\delta f^a|_{p^\mu} = gV^\alpha F^a_{\alpha\beta}\partial^\beta_{(p)} f_0(\mathbf{p}_\perp, p_\eta), \tag{2.13}$$

where in place of the lightlike vector $v^\mu = p^\mu/p^0$ containing a unit 3-vector we introduced the new quantity

$$V^\alpha = \frac{p^\alpha}{p_\perp} = \Big(\cosh(y-\eta), \cos\phi, \sin\phi, \frac{1}{\tau}\sinh(y-\eta)\Big), \tag{2.14}$$

which is normalized so that it has a unit 2-vector in the transverse plane.

Equation (2.13) can be solved in terms of an auxiliary field $W_\beta(x; \phi, y)$ which satisfies

$$V\cdot DW_\beta|_{\phi,y} = V^\alpha F_{\beta\alpha}, \tag{2.15}$$

and

$$\delta f(x; p) = -gW_\beta(x; \phi, y)\partial^\beta_{(p)} f_0(p_\perp, p_\eta). \tag{2.16}$$

Expressed in terms of the auxiliary field W, the induced current in comoving coordinates reads

$$j^\alpha = g t_R \int \frac{d^3p}{(2\pi)^3 2p^0} p^\alpha \delta f(x;p)$$
$$= -g^2 t_R \int_0^\infty \frac{p_\perp dp_\perp}{8\pi^2} \int_0^{2\pi} \frac{d\phi}{2\pi} \times \int_{-\infty}^{\infty} dy p^\alpha \frac{\partial f_0}{\partial p_\beta} W_\beta(x;\phi,y), \quad (2.17)$$

where t_R is a suitably normalized group factor. Now for each (ϕ, y) (i.e., fixed $\mathbf{v}$) the scale $p_\perp$ (related to energy by $p^0 = p_\perp \cosh y$) can be integrated out.

With the particular background distribution function (2.10) we obtain

$$j^\alpha = -m_D^2 \frac{1}{2} \int_0^{2\pi} \frac{d\phi}{2\pi} \int_{-\infty}^{\infty} dy V^\alpha \left(1 + \frac{\tau^2}{\tau_{\rm iso}^2} \sinh^2(y-\eta)\right)^{-2} \times \left(V^i W_i + \frac{\tau^2}{\tau_{\rm iso}^2} V^\eta W_\eta\right), \quad (2.18)$$

where

$$m_D^2 = -g^2 t_R \int_0^\infty \frac{dp p^2}{(2\pi)^2} f'_{\rm iso}(p) \quad (2.19)$$

equals the Debye mass squared at the time $\tau_{\rm iso}$ (which we shall often choose smaller than τ_0 so that m_D is not physically realized by just a convenient mass parameter).

These equations are closed by the non-Abelian Maxwell equations which in comoving coordinates read

$$\frac{1}{\tau} D_\alpha(\tau F^{\alpha\beta}) \equiv \frac{1}{\tau} D_\alpha[\tau g^{\alpha\gamma}(\tau) g^{\beta\delta}(\tau) F_{\gamma\delta}] = j^\beta, \quad (2.20)$$

where $F_{\alpha\beta} = \partial_\alpha A_\beta - \partial_\beta A_\alpha - ig[A_\alpha, A_\beta]$. To solve them, we adopt the comoving temporal gauge $A^\tau = 0$ and introduce canonical conjugate field momenta for the remaining gauge fields according to[2]

$$\Pi^i = \tau \partial_\tau A_i = -\tau \partial_\tau A^i = -\Pi_i, \quad (2.21)$$

and

$$\Pi^\eta = \frac{1}{\tau} \partial_\tau A_\eta. \quad (2.22)$$

In terms of fields and conjugate momenta, the Yang-Mills field equations then read

$$\tau \partial_\tau \Pi^\eta = j_\eta - D_i F^i{}_\eta, \quad (2.23)$$

$$\tau^{-1} \partial_\tau \Pi_i = j^i - D_j F^{ji} - D_\eta F^{\eta i}. \quad (2.24)$$

In a comoving frame, the longitudinal (chromo)electric and magnetic fields are given by

$$E^\eta = \Pi^\eta, \qquad B_\eta = F_{12}, \quad (2.25)$$

but transverse components involve a factor of τ,

$$E^i = \tau^{-1} \Pi^i, \qquad B_i = \tau^{-1} F_{\eta j} \epsilon_{ji}. \quad (2.26)$$

In terms of these, the contribution to the energy density is simply

$$\mathcal{E} = \mathcal{E}_T + \mathcal{E}_L = \mathcal{E}_{B_T} + \mathcal{E}_{E_T} + \mathcal{E}_{B_L} + \mathcal{E}_{E_L}$$
$$= \mathrm{tr}[(B_i)^2 + (E^i)^2 + (B_\eta)^2 + (E^\eta)^2]. \quad (2.27)$$

However, due to the expansion, the total energy density $\mathcal{E}$ is not conserved, even when the induced current (2.17) is identically zero,

$$\frac{d}{d\tau} \mathcal{E}|_{j\equiv 0} = -\frac{2}{\tau} \mathcal{E}_T|_{j\equiv 0}. \quad (2.28)$$

In the presence of a plasma of hard particles and thus nonvanishing induced current j, we define the net energy gain rate by

$$R_{\rm gain} \equiv \frac{d\mathcal{E}}{d\tau} + \frac{2}{\tau} \mathcal{E}_T, \quad (2.29)$$

which gives the rate of energy transfer from the free-streaming hard particles into the collective chromofields and which is positive when plasma instabilities are at work. For stable modes $R_{\rm gain}$ oscillates about zero.

III. TIME EVOLUTION OF GAUGE FIELDS IN THE WEAK-FIELD REGIME

In the regime where self-interactions of gauge fields cannot be neglected, the Yang-Mills field equations and the equations of motion for the $W_\alpha(x;\phi,y)$ fields are nonlinear and require numerical, real-time lattice evaluation. In the limit of small field amplitudes, these equations are linear and can be reduced to ordinary integrodifferential equations in proper time for individual modes.

A. Solving the W field equations

In the weak-field regime, the W field equations reduce to

$$(V^\tau \partial_\tau + V^i \partial_i + V^\eta \partial_\eta) W_\alpha(\tau, x^i, \eta; \phi, y) = V^\beta F_{\alpha\beta} = V^\beta (\partial_\alpha A_\beta - \partial_\beta A_\alpha). \quad (3.1)$$

Because our background distribution function is isotropic in the transverse plane, we can without loss of generality restrict to modes which are independent of $x^{i=2}$, keeping only $x^{i=1} \equiv x$ (recall that the symbol y is already used for momentum rapidity). In temporal axial gauge we thus have

$$(V^\tau \partial_\tau + V^\eta \partial_\eta + \cos\phi \partial_x) W_\alpha(\tau, x, \eta; \phi, y) = -V^\tau \partial_\tau A_\alpha + V^\eta (\partial_\alpha A_\eta - \partial_\eta A_\alpha) + \cos\phi (\partial_\alpha A_1 - \partial_x A_\alpha) + \sin\phi \partial_\alpha A_2. \quad (3.2)$$

These first-order partial differential equations can be solved by the method of characteristics as follows. We introduce a parameter s such that the left-hand side of Eq. (3.2) is replaced by

[2] In the following field equations we keep the index position of conjugate field momenta opposite to that of the associated fields.

$$\frac{dW_\alpha}{ds} = \frac{\partial W_\alpha}{\partial \tau}\frac{d\tau}{ds} + \frac{\partial W_\alpha}{\partial \eta}\frac{d\eta}{ds} + \frac{\partial W_\alpha}{\partial x}\frac{dx}{ds} \tag{3.3}$$

with

$$\frac{d\tau}{ds} = V^\tau = \cosh(y - \eta(s)), \tag{3.4}$$

$$\frac{d\eta}{ds} = V^\eta = \frac{1}{\tau(s)}\sinh(y - \eta(s)), \tag{3.5}$$

$$\frac{dx}{ds} = V^1 = \cos\phi. \tag{3.6}$$

Since $d\tau/ds > 0$ we can use τ in place of s for the purpose of integrating Eq. (3.2). Writing $ds = d\tau'/V^\tau(\eta(\tau'))$ we obtain

$$W_\alpha(\tau, x, \eta; \phi, y) - W_\alpha(\tau_0, x_0, \eta_0; \phi, y) = \int_{\tau_0}^{\tau} d\tau' \frac{V^\beta F_{\alpha\beta}|_{\tau', x(\tau'), \eta(\tau')}}{\cosh(y - \eta(\tau'))} \tag{3.7}$$

with $x_0 \equiv x(\tau' = \tau_0)$ and $\eta_0 \equiv \eta(\tau' = \tau_0)$. The functions $\eta(\tau')$ and $x(\tau')$ are solutions of

$$\frac{d\eta(\tau')}{d\tau'} = \frac{1}{\tau'}\tanh(y - \eta(\tau')) \tag{3.8}$$

$$\frac{dx(\tau')}{d\tau'} = \frac{\cos\phi}{\cosh(y - \eta(\tau'))} \tag{3.9}$$

with initial conditions $\eta(\tau' = \tau) = \eta$ and $x(\tau' = \tau) = x$. Equation (3.8) is solved by [39]

$$\tau' \sinh(y - \eta(\tau')) = \tau \sinh(y - \eta) \tag{3.10}$$

or, more explicitly,

$$\eta' \equiv \eta(\tau') = y - \operatorname{asinh}\left(\frac{\tau}{\tau'}\sinh(y - \eta)\right). \tag{3.11}$$

With this solution, Eq. (3.9) can be integrated, yielding

$$x' \equiv x(\tau') = x + [\tau' \cosh(y - \eta') - \tau \cosh(y - \eta)]\cos\phi. \tag{3.12}$$

The W fields, from which the induced current is obtained upon integration over ϕ and y according to Eq. (2.18), are now given explicitly by the following "memory integrals":

$$\begin{aligned}
W_1 - W_1^0 &= \int_{\tau_0}^{\tau} d\tau' \Big[\partial_{\tau'} A^1 - \frac{\tanh(\eta' - y)}{\tau'} \\
&\quad \times (\partial_{x'} A_\eta + \partial_{\eta'} A^1) - \frac{\sin\phi}{\cosh(\eta' - y)}\partial_{x'} A^2 \Big], \\
W_2 - W_2^0 &= \int_{\tau_0}^{\tau} d\tau' \Big[\partial_{\tau'} - \frac{\tanh(\eta' - y)}{\tau'}\partial_{\eta'} \\
&\quad + \frac{\cos\phi}{\cosh(\eta' - y)}\partial_{x'} \Big] A^2, \\
W_\eta - W_\eta^0 &= -\int_{\tau_0}^{\tau} d\tau' \Big[\partial_{\tau'} A_\eta + \frac{V^i \partial_{\eta'} A^i + \partial_{x'} A_\eta}{\cosh(\eta' - y)} \Big],
\end{aligned} \tag{3.13}$$

where inside the integrals $A_\alpha = A_\alpha(\tau', x', \eta')$. Note that x' and η' as well as x_0 and η_0 appearing as arguments in $W_\alpha^0 \equiv W_\alpha(\tau_0, x_0, \eta_0; \phi, y)$ all are functions of the space-time variables τ, η, and x.

B. Fourier components

Because of the linearity of the Maxwell (linearized Yang-Mills) equations and the W equations in the weak-field (Abelian) regime and their translational invariance in η and y, we can study the time evolution of individual modes obtained by a Fourier decomposition

$$A_\alpha(\tau, x, \eta) = \int \frac{dk}{2\pi} e^{ikx} \int \frac{d\nu}{2\pi} e^{i\nu\eta} \tilde{A}_\alpha(\tau; k, \nu). \tag{3.14}$$

With similarly Fourier transformed currents, the equations of motion for $\tilde{A}^1$ and $\tilde{A}_\eta$ read

$$\begin{aligned}
(\tau^{-1}\partial_\tau \tau \partial_\tau + \tau^{-2}\nu^2)\tilde{A}^1(\tau; k, \nu) &= \tilde{j}^1(\tau; k, \nu) - k\nu\tau^{-2}\tilde{A}_\eta(\tau; k, \nu) \\
(\tau\partial_\tau\tau^{-1}\partial_\tau + k^2)\tilde{A}_\eta(\tau; k, \nu) &= \tilde{j}_\eta(\tau; k, \nu) - k\nu\tilde{A}^1(\tau; k, \nu)
\end{aligned} \tag{3.15}$$

with $\tilde{j}^1(\tau; k, \nu)$ and $\tilde{j}_\eta(\tau; k, \nu)$ both depending on $\tilde{A}^1(\tau'; k, \nu)$ and $\tilde{A}_\eta(\tau'; k, \nu)$, $\tau' \le \tau$, but not on $\tilde{A}^2(\tau'; k, \nu)$, as we shall see shortly. The equation of motion for the transverse mode $\tilde{A}^2(\tau; k, \nu)$ is decoupled from $\tilde{A}^1$ and $\tilde{A}_\eta$ and reads

$$(\tau^{-1}\partial_\tau\tau\partial_\tau + k^2 + \tau^{-2}\nu^2)\tilde{A}^2(\tau; k, \nu) = \tilde{j}^2(\tau; k, \nu) \tag{3.16}$$

with $\tilde{j}^2(\tau; k, \nu)$ depending on the history of $\tilde{A}^2(\tau'; k, \nu)$.

In order to express the current as functional of the gauge fields, we first note that in Eqs. (3.13), the partial derivatives $\partial_{x'}$ and $\partial_{\eta'}$ are simply replaced by factors ik and $i\nu$, respectively, while the proper-time integrals over the *partial* time derivative of the gauge fields $A_\alpha(\tau', x', \eta')$ can be integrated by parts, yielding

$$\int_{\tau_0}^{\tau} d\tau' \partial_{\tau'} A_\alpha(\tau', x', \eta') = \int_{\tau_0}^{\tau} d\tau' \int \frac{dk}{2\pi} e^{ikx'(\tau')} \int \frac{d\nu}{2\pi} e^{i\nu\eta'(\tau')} \partial_{\tau'} \tilde{A}_\alpha(\tau; k, \nu)$$
$$= \int \frac{dk}{2\pi} \int \frac{d\nu}{2\pi} \Big\{ e^{ikx} e^{i\nu\eta} \tilde{A}_\alpha(\tau; k, \nu) - e^{ikx_0(\tau)} e^{i\nu\eta_0(\tau)} \tilde{A}_\alpha(\tau_0; k, \nu)$$
$$- i \int_{\tau_0}^{\tau} d\tau' e^{ikx'} e^{i\nu\eta'} \Big[k \frac{\cos\phi}{\cosh(y-\eta')} + \nu \frac{\tanh(y-\eta')}{\tau'} \Big] \tilde{A}_\alpha(\tau'; k, \nu) \Big\}. \tag{3.17}$$

Inserting Eqs. (3.13) with (3.17) into the expression for the current, Eq. (2.18) and introducing the abbreviations[3]

$$\bar{y} \equiv y - \eta, \qquad \bar{\eta}' \equiv \bar{\eta}(\tau') \equiv \eta(\tau') - \eta = \bar{y} - \operatorname{asinh}\Big(\frac{\tau}{\tau'} \sinh\bar{y}\Big), \qquad \bar{\eta}_0 \equiv \bar{\eta}(\tau_0),$$
$$\bar{\chi}' \equiv \bar{\chi}(\tau') \equiv (x(\tau') - x)/\cos\phi = \sqrt{\tau'^2 + \tau^2 \sinh^2\bar{y}} - \tau\cosh\bar{y}, \qquad \bar{\chi}_0 \equiv \bar{\chi}(\tau_0), \tag{3.18}$$

we find the following results for the Fourier components $\tilde{j}^\alpha(\tau; k, \nu)$ after performing the integration over the (momentum-space) angle ϕ in terms of Bessel functions J_n,

$$\tilde{j}^1 = -\frac{m_D^2}{2} \int \frac{d\bar{y}}{(1 + \frac{\tau^2\sinh^2\bar{y}}{\tau_{\rm iso}^2})^2} \Big\{ \frac{1}{2}\tilde{A}^1(\tau) + e^{i\nu\bar{\eta}_0} \Big[\frac{i\tau\sinh\bar{y}}{\tau_{\rm iso}^2} J_1(k\bar{\chi}_0)\tilde{A}_\eta(\tau_0) - \frac{1}{2}[J_0 - J_2](k\bar{\chi}_0)\tilde{A}^1(\tau_0) \Big]$$
$$+ \int_{\tau_0}^{\tau} d\tau' \frac{e^{i\nu\bar{\eta}'}}{\sqrt{1 + \frac{\tau^2\sinh^2\bar{y}}{\tau'^2}}} \Big[\Big(\frac{k}{4}[3J_1 - J_3](k\bar{\chi}') - \frac{i\nu\tau\sinh\bar{y}}{2\tau_{\rm iso}^2}[J_0 - J_2](k\bar{\chi}') \Big) \tilde{A}^1(\tau')$$
$$+ \frac{\tau\sinh\bar{y}}{\tau'^2} \Big(\frac{ik}{2}[J_0 - J_2](k\bar{\chi}') - \frac{\nu\tau\sinh\bar{y}}{\tau_{\rm iso}^2} J_1(k\bar{\chi}') \Big) \tilde{A}_\eta(\tau') \Big] \Big\} + \tilde{j}_0^1(\tau), \tag{3.19}$$

and

$$\tilde{j}^\eta = -\frac{m_D^2}{2\tau} \int \frac{d\bar{y}\sinh\bar{y}}{(1 + \frac{\tau^2\sinh^2\bar{y}}{\tau_{\rm iso}^2})^2} \Big\{ -\frac{\tau\sinh\bar{y}}{\tau_{\rm iso}^2} \tilde{A}_\eta(\tau) + e^{i\nu\bar{\eta}_0} \Big[\frac{\tau\sinh\bar{y}}{\tau_{\rm iso}^2} J_0(k\bar{\chi}_0)\tilde{A}_\eta(\tau_0) - iJ_1(k\bar{\chi}_0)\tilde{A}^1(\tau_0) \Big] + \int_{\tau_0}^{\tau} d\tau' \frac{e^{i\nu\bar{\eta}'}}{\sqrt{1 + \frac{\tau^2\sinh^2\bar{y}}{\tau'^2}}}$$
$$\times \Big[\Big(\frac{ik}{2}[J_2 - J_0](k\bar{\chi}') + \frac{\nu\tau\sinh\bar{y}}{\tau_{\rm iso}^2} J_1(k\bar{\chi}') \Big) \tilde{A}^1(\tau') + \frac{\tau\sinh\bar{y}}{\tau'^2} \Big(\frac{i\nu\tau\sinh\bar{y}}{\tau_{\rm iso}^2} J_0(k\bar{\chi}') - kJ_1(k\bar{\chi}') \Big) \tilde{A}_\eta(\tau') \Big] \Big\} + \tilde{j}_0^\eta(\tau). \tag{3.20}$$

As mentioned above, these components of the current only depend on (the history of) $\tilde{A}^1$ and $\tilde{A}_\eta$. If either $k = 0$ or $\nu = 0$, the 1 and η components decouple from each other. [For $k = 0$ only the terms involving $J_0(0) = 1$ survive, while for $\nu = 0$ all terms involving odd powers of $\sinh\bar{y}$ integrate to zero.] On the other hand, $\tilde{j}^2$ is found to be a functional of only $\tilde{A}^2$,

$$\tilde{j}^2 = -\frac{m_D^2}{4} \int \frac{d\bar{y}}{(1 + \frac{\tau^2\sinh^2\bar{y}}{\tau_{\rm iso}^2})^2} \Big\{ \tilde{A}^2(\tau) - e^{i\nu\bar{\eta}_0}[J_0 + J_2](k\bar{\chi}_0)$$
$$\times \tilde{A}^2(\tau_0) + \int_{\tau_0}^{\tau} d\tau' \frac{e^{i\nu\bar{\eta}'}}{\sqrt{1 + \frac{\tau^2\sinh^2\bar{y}}{\tau'^2}}} \Big(\frac{k}{2}[J_1 + J_3](k\bar{\chi}')$$
$$- \frac{i\nu\tau\sinh\bar{y}}{\tau_{\rm iso}^2}[J_0 + J_2](k\bar{\chi}') \Big) \tilde{A}^2(\tau') \Big\} + \tilde{j}_0^2(\tau). \tag{3.21}$$

Equations (3.19), (3.20), and (3.21) generalize the expressions given in [39] for the effectively $1 + 1$-dimensional case $k = 0$, where the wave vector of the collective modes points in the direction of momentum-space anisotropy. (As they should, the functional dependences in $\tilde{j}^1[\tilde{A}^1]$ and $\tilde{j}^2[\tilde{A}^2]$ become the same for $k = 0$.)

The τ component of the current, which is needed only for a check of the Gauss law constraint, is again independent of $\tilde{A}^2$ and given by the following functional of $\tilde{A}^1$ and $\tilde{A}_\eta$:

$$\tilde{j}^\tau = -\frac{m_D^2}{2} \int \frac{d\bar{y}\cosh\bar{y}}{(1 + \frac{\tau^2\sinh^2\bar{y}}{\tau_{\rm iso}^2})^2} \Big\{ e^{i\nu\bar{\eta}_0} \Big[\frac{\tau\sinh\bar{y}}{\tau_{\rm iso}^2} J_0(k\bar{\chi}_0)\tilde{A}_\eta(\tau_0)$$
$$- iJ_1(k\bar{\chi}_0)\tilde{A}^1(\tau_0) \Big] + \int_{\tau_0}^{\tau} d\tau' \frac{e^{i\nu\bar{\eta}'}}{\sqrt{1 + \frac{\tau^2\sinh^2\bar{y}}{\tau'^2}}}$$
$$\times \Big[\Big(\frac{ik}{2}[J_2 - J_0](k\bar{\chi}') + \frac{\nu\tau\sinh\bar{y}}{\tau_{\rm iso}^2} J_1(k\bar{\chi}') \Big) \tilde{A}^1(\tau')$$
$$+ \frac{\tau\sinh\bar{y}}{\tau'^2} \Big(\frac{i\nu\tau\sinh\bar{y}}{\tau_{\rm iso}^2} J_0(k\bar{\chi}') - kJ_1(k\bar{\chi}') \Big) \tilde{A}_\eta(\tau') \Big] \Big\}$$
$$+ \tilde{j}_0^\tau(\tau). \tag{3.22}$$

[3]The notation is chosen such that a bar indicates a dependence on $\bar{y}$ and a prime a dependence on τ' [$\bar{y}$ and τ' are the two remaining integration variables in Eqs. (3.19), (3.20), (3.21), and (3.22)].

In all these expressions, $\tilde{j}_0^\alpha(\tau; k, \nu)$ corresponds to nontrivial initial data for W_α, if any. Up to a factor $e^{ikx}e^{i\nu\eta}$, the Fourier component $\tilde{j}_0^\alpha(\tau; k, \nu)$ is obtained by evaluating the expression for the induced current, Eq. (2.18), with W's of the form

$$W_\alpha(\tau_0, x_0(\tau), \eta_0(\tau); \phi, y) = e^{ikx_0(\tau)}e^{i\nu\eta_0(\tau)} \times \tilde{W}_\alpha^0(k, \nu; \phi, y - \eta_0(\tau)), \tag{3.23}$$

where the functions x_0 and η_0 are given by Eqs. (3.12) and (3.11), respectively, with $\tau' = \tau_0$. Nontrivial initial values $\tilde{W}_\alpha^0$ are required whenever the right-hand side of the Gauss law constraint at $\tau = \tau_0$,

$$\tilde{j}^\tau(\tau_0) = \frac{i}{\tau_0}(\nu\tilde{\Pi}^\eta(\tau_0) + k\tilde{\Pi}^1(\tau_0)), \tag{3.24}$$

is nonvanishing. This is naturally the case for modes where the polarization of the gauge fields and their momenta (in temporal gauge) is longitudinal with respect to the spatial wave vector.

Note that already for a single mode there is considerable freedom in the choice of initial conditions which is parametrized by the functions $\tilde{W}_\alpha^0(k, \nu; \phi, y - \eta_0)$ and which will be explored in detail below.

C. Stable and unstable modes

Before studying the time evolution of the individual Fourier modes through numerical evaluation of the integrodifferential equations provided by the above expressions, it is useful to recall the case of a stationary anisotropic plasma, where a rather complete analysis of stable and unstable modes in the regime of weak fields has been carried out in Refs. [8,28,29]. This is still relevant for the expanding case, which is however complicated by the time dependence of the density of the plasma and its anisotropy parameter so that some unstable modes may shut off as the plasma evolves towards a higher degree of oblateness, while new ones come into being. Since the growth rate of unstable modes also depends on the orientation of the wave vector, a further complication comes from the fact that this orientation is time dependent unless the wave vector is strictly parallel or orthogonal to the anisotropy direction. When both $k \neq 0$ and $\nu \neq 0$, in comoving Cartesian coordinates the wave vector rotates into the transverse plane according to

$$\mathbf{k} = k\mathbf{e}_1 + \frac{\nu}{\tau}\mathbf{e}_3 \tag{3.25}$$

with the angle between $\mathbf{k}$ and $\mathbf{e}_3$ given by

$$\vartheta = \arctan\frac{\tau k}{\nu}. \tag{3.26}$$

When the anisotropy is characterized by only one spatial direction, as is the case for the distribution (2.10), there are in general three different branches[4] of modes. Following Ref. [28], the modes with a polarization of the electric field transverse to both wave vector and the direction of anisotropy are denoted by the label α. In our case these correspond to the Fourier components $\tilde{A}^2(\tau; k, \nu)$ and $\tilde{j}^2(\tau; k, \nu)$, described by Eqs. (3.16) and (3.21). Such modes are stable in the case of a prolate momentum anisotropy, and unstable for all orientations of the wave vector in the case of oblate anisotropy, but the growth rate of the latter approaches zero as $\vartheta \to \frac{\pi}{2}$. In the terminology of Ref. [8], these instabilities are magnetic ones and have been first described by Weibel [45]. The instabilities studied so far for expanding plasmas [39,40] correspond to such modes in the special case $\vartheta = 0$.

When the polarization of the electric field (and of the gauge field in temporal gauge) lies in the plane spanned by the wave vector and the direction of anisotropy, there are two modes, labeled "+" and "−" in Ref. [28], according to which one has the larger (+) or smaller (−) zero-frequency mass squared in the stationary anisotropic case. In the isotropic case, the "+" mode corresponds to electric Debye screening at zero frequency and longitudinal plasmons above the plasma frequency, whereas the "−" mode coincides with the α mode (which in this case has zero screening mass to leading order). In the anisotropic case, this degeneracy is lifted as soon as $\vartheta \neq 0$. Now the "−" mode is unstable for both oblate and prolate anisotropies, but in each case for only a limited range of angles ϑ, see Table I.

For generic orientation of the wave vector, the "−" mode involves also longitudinal electric fields and thus can correspond to an electric instability according to the classification of Ref. [8]. However, when either $k = 0$ ($\vartheta = 0$) or $\nu = 0$ ($\vartheta = \frac{\pi}{2}$), the equations for $\tilde{A}^1$ and $\tilde{A}_\eta$, (3.15), (3.19), and (3.20), decouple. The mode which is longitudinal with respect to $\mathbf{k}$ is then electrically screened, whereas the other one is transverse and corresponds to either magnetostatic screening (when $\vartheta = \frac{\pi}{2}$ in the oblate case, or $\vartheta = 0$ in the prolate case), or a magnetic instability (when $\vartheta = 0$ in the oblate case, or $\vartheta = \frac{\pi}{2}$ in the prolate case).[5]

In the following we shall study the time evolution of some representative cases of stable and unstable modes in the expanding case, for initially oblate as well as prolate anisotropies, with a particular view on the dependence on initial conditions.

[4]For a given wave vector, one branch may have more than one mode, e.g., a propagating wave and a growing unstable mode.

[5]For large anisotropies, the magnetostatic screening mass may even become larger than the electrostatic (Debye) mass, e.g. with prolate anisotropy $\xi \lesssim -0.88$, as is the case in Fig. 2b of Ref. [28], whereupon electrostatic Debye screening at $\vartheta = 0$ becomes part of the "−" branch and thus continuously connected with the magnetic instability at $\vartheta = \frac{\pi}{2}$.

TABLE I. Classification of modes according to Ref. [28], the corresponding polarization of the electric and magnetic field, and the range of instabilities in terms of the angle ϑ between the wave vector $\mathbf{k}$ and the direction of anisotropy ($\mathbf{e}_3$).

Mode	E field	B field	Instabilities, prolate case	Instabilities, oblate case
α	$\mathbf{k}\perp\mathbf{E}\parallel\mathbf{e}_2$	$\mathbf{k}\perp\mathbf{B}\perp\mathbf{e}_2$	Stable	$0\le\vartheta<\frac{\pi}{2}$
$+$	$\mathbf{E}\perp\mathbf{e}_2$	$\mathbf{k}\perp\mathbf{B}\parallel\mathbf{e}_2$	Stable	Stable
$-$	$\mathbf{E}\perp\mathbf{e}_2$	$\mathbf{k}\perp\mathbf{B}\parallel\mathbf{e}_2$	$\frac{\pi}{4}\lesssim\vartheta\le\frac{\pi}{2}$	$0\le\vartheta\lesssim\frac{\pi}{4}$

IV. NUMERICAL EVALUATION

The integrodifferential equations for the time evolution of individual Fourier modes that we have obtained in Sec. III B for the linear-response regime can be solved straightforwardly by discretizing the proper time variables τ and employing a leap frog algorithm for gauge fields and conjugate momenta, Eqs. (2.21), (2.22), (2.23), and (2.24). The memory integrals in the expressions for the induced currents also involve integrations over the momentum rapidity variable $\bar{y}$ that have to be performed for each time step between τ_0 and τ.

Since we are interested in the earliest stage of the evolution of plasma instabilities from small initial fluctuations, we choose our dimensionful quantities such that $\tau_0\sim Q_s$, with Q_s the so-called saturation scale of the color-glass-condensate (CGC) framework [41,46], and a normalization of the hard particle distribution function (2.10) such that at $\tau=\tau_0$ the hard-gluon density of CGC estimates is matched. This involves the so-called gluon liberation factor c [47], which we choose as $c=2\ln 2\approx 1.386$ as obtained in approximate analytical calculations by Kovchegov in Ref. [48]. While this value is significantly larger than the first numerical estimates [49,50], it is fairly close to the most recent numerical result $c\simeq 1.1$ by Lappi [51]. Our choice of c corresponds to a value of the squared mass parameter m_D^2 in the expression for the induced current of $m_D^2\approx 1.285(\tau_0\tau_{\rm iso})^{-1}$. (See Appendix C of Ref. [40] for details.) Unless stated otherwise, this value will be used in the following numerical calculations. The only remaining free parameter is then $\tau_{\rm iso}$, parametrizing the amount of anisotropy at the initial time τ_0, and we shall consider both initially prolate and oblate distributions.

For later reference we note that if we assume $\tau_0^{-1}\sim Q_s\sim 1$ and 3 GeV for RHIC and LHC experiments, respectively, 1 fm/c corresponds to $\sim 5\tau_0$ for RHIC and $\sim 15\tau_0$ for LHC.

A. Wave vector parallel to anisotropy direction

Fourier modes with $k=0$ and $\nu\neq 0$ have a wave vector parallel to the spatial direction of momentum anisotropy and thus are constant in the plane transverse to the axis of expansion. Such modes are stable for prolate anisotropy, while with oblate anisotropy there are magnetic (Weibel) instabilities below a certain (ξ- or τ-dependent) value of ν. The case $k=0$, which has been studied semianalytically before in Ref. [39], is particularly interesting since it covers the most unstable mode of a plasma with oblate anisotropy.

Before studying the unstable modes in more detail (eventually also with $k\neq 0$), we begin with the stable longitudinal modes, which are complicated by the need for nonvanishing initial induced currents. The analysis of Ref. [39] of the unstable modes at $k=0$ will then be generalized by allowing also for nonvanishing initial currents.

1. Stable (longitudinal plasmon) modes

Longitudinal modes with $k=0$ and nonvanishing A_η, Π^η are purely electrical and correspond to charge density waves (longitudinal plasmons). Initial conditions only in A_η, with zero initial Π^η and W fields, would only yield a trivial, constant solution. For nontrivial solutions, we need nonvanishing initial W fields and nonzero initial currents. In order to have nonzero $\tilde{j}^\tau(\tau_0;\nu)$ we need initial values of the W fields that are odd in $\bar{y}\equiv y-\eta$. A possible choice is

$$\tilde{W}^{\,0}_{\eta}(k=0,\nu;\phi,y-\eta_0)=C_1\tanh(y-\eta_0), \tag{4.1}$$

where C_1 is a constant. We recall that η_0 is given by (3.11) as

$$\eta_0\equiv\eta(\tau'=\tau_0)=y-\operatorname{asinh}\!\left(\frac{\tau}{\tau_0}\sinh(y-\eta)\right) \tag{4.2}$$

so that $\eta_0=\eta$ at $\tau=\tau_0$. The Gauss law constraint (3.24) relates the constant C_1 to the initial value of the longitudinal electric field according to

$$\tilde{j}^{\,\tau}(\tau_0;\nu)=-\frac{2\pi C_1 m_D^2\tau_0}{2\tau_{\rm iso}^2}\int\frac{d\bar{y}\sinh^2\bar{y}}{(1+\frac{\tau_0^2\sinh^2\bar{y}}{\tau_{\rm iso}^2})^2}=\frac{i\nu\tilde{\Pi}^\eta(\tau_0;\nu)}{\tau_0}. \tag{4.3}$$

The nonzero W^0_η field (4.1) thus gives rise to the following contributions $\tilde{j}^\alpha_0(\tau)$ in the integral equations (3.20) and (3.22):

$$\tilde{j}^{\,\tau}_0(\tau;\nu)=\frac{i\nu\tau^2\tilde{\Pi}^\eta(\tau_0;\nu)}{\tau_0^3}N^{-1}\int\frac{d\bar{y}e^{i\nu\bar{\eta}_0}\cosh\bar{y}\sinh^2\bar{y}}{(1+\frac{\tau^2\sinh^2\bar{y}}{\tau_{\rm iso}^2})^2\sqrt{1+\frac{\tau^2\sinh^2\bar{y}}{\tau_0^2}}}, \tag{4.4}$$

$$\tilde{j}^{\eta}_0(\tau;\nu) = \frac{i\nu\tau\tilde{\Pi}^{\eta}(\tau_0;\nu)}{\tau_0^3} N^{-1} \int \frac{d\bar{y} e^{i\nu\bar{\eta}_0}\sinh^3\bar{y}}{(1+\frac{\tau^2\sinh^2\bar{y}}{\tau_{\rm iso}^2})^2\sqrt{1+\frac{\tau^2\sinh^2\bar{y}}{\tau_0^2}}}, \tag{4.5}$$

where[6]

$$N(\tau_{\rm iso}/\tau_0) = \int \frac{d\bar{y}\sinh^2\bar{y}}{(1+\frac{\tau_0^2\sinh^2\bar{y}}{\tau_{\rm iso}^2})^2}. \tag{4.6}$$

Recall that $\bar{\eta}_0 \equiv \eta_0 - \eta$, which vanishes at $\tau = \tau_0$, so that $\tilde{j}^{\eta}_0(\tau_0;\nu) = 0$.

With $k = 0$, the complete expression for the induced current (3.20) reads

$$\begin{aligned}\tilde{j}^{\eta}(\tau;\nu) = \frac{m_D^2}{2\tau_{\rm iso}^2}\int \frac{d\bar{y}\sinh^2\bar{y}}{(1+\frac{\tau^2\sinh^2\bar{y}}{\tau_{\rm iso}^2})^2}\Big\{&\tilde{A}_{\eta}(\tau;\nu) \\ &- e^{i\nu\bar{\eta}_0}\tilde{A}_{\eta}(\tau_0;\nu) \\ &- \int_{\tau_0}^{\tau} d\tau' \frac{i\nu\tau e^{i\nu\bar{\eta}'}\sinh\bar{y}}{\tau'^2\sqrt{1+\frac{\tau^2\sinh^2\bar{y}}{\tau_{\rm iso}}}}\tilde{A}_{\eta}(\tau';\nu)\Big\} \\ &+ \tilde{j}^{\tau}_0(\tau;\nu),\end{aligned} \tag{4.7}$$

which has to be solved together with

$$\partial_\tau \frac{1}{\tau}\partial_\tau A_{\eta}(\tau;\nu) = -\tau\tilde{j}^{\eta}(\tau;\nu). \tag{4.8}$$

In Appendix A 2 the late-time behavior of the solutions is derived in terms of Bessel functions J_2 and Y_2, see Eq. (A18). In Fig. 1 this is compared with results of a full numerical solution of the above integrodifferential equation for $\tilde{A}_{\eta}$ using $\tau_{\rm iso}/\tau_0 = 10$ so that the time evolution starts in the prolate phase, and $\nu = 0$ and 1. The late-time (large oblate anisotropy) behavior is reproduced very well, with noticeable deviations at earlier times.

2. Unstable (transverse) modes

With $k = 0$, there are two degenerate transverse modes described by the then coinciding equations (3.19) and (3.21) for the induced currents $\tilde{j}^1$ and $\tilde{j}^2$, which reduce to

$$\begin{aligned}\tilde{j}^{i}(\tau;\nu) = -\frac{m_D^2}{4}\int \frac{d\bar{y}}{(1+\frac{\tau^2\sinh^2\bar{y}}{\tau_{\rm iso}^2})^2}\Big\{&\tilde{A}^{i}(\tau;\nu) \\ &- e^{i\nu\bar{\eta}_0}\tilde{A}^{i}(\tau_0;\nu) \\ &- \int_{\tau_0}^{\tau} d\tau' \frac{i\nu\tau e^{i\nu\bar{\eta}'}\sinh\bar{y}}{\tau_{\rm iso}^2\sqrt{1+\frac{\tau^2\sinh^2\bar{y}}{\tau'^2}}}\tilde{A}^{i}(\tau';\nu)\Big\} \\ &+ \tilde{j}^{i}_0(\tau;\nu).\end{aligned} \tag{4.9}$$

This has to be solved together with

[6]See Eq. (A13) for an analytic expression for N.

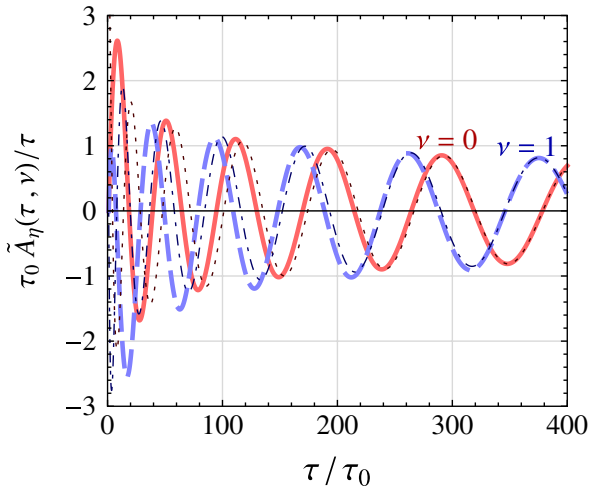

FIG. 1 (color online). Longitudinal modes with $\nu = 0$ and 1 for $\tau_{\rm iso}/\tau_0 = 10$. The dotted and dash-dotted lines represent the analytic results for the late-time behavior, Eq. (A18), which are in good agreement with the numerical data (thick full lines) at sufficiently large times.

$$\begin{aligned}\tilde{\Pi}_i(\tau;\nu) &= \tau\partial_\tau A^i, \\ \frac{1}{\tau}\partial_\tau\tilde{\Pi}_i(\tau;\nu) &= \tilde{j}^{i}(\tau;\nu) - \frac{\nu^2}{\tau^2}\tilde{A}^{i}(\tau;\nu).\end{aligned} \tag{4.10}$$

In the notation of Table I, the solutions of these equations correspond to the modes "$-$" and "α," which become the same at $\vartheta = 0$. This case, which contains magnetic Weibel instabilities for oblate anisotropies, was studied already in Ref. [39], but with vanishing initial W fields and, correspondingly, vanishing initial currents, which now is perfectly consistent with the Gauss law constraint $\tilde{j}^{\tau} \propto \tilde{\Pi}^{\eta} = 0$.

In the following numerical evaluations we shall be more general and consider separately the initial conditions of (i) a seed electric field with only $\tilde{\Pi}^{i}(\tau_0) \neq 0$, which is the case studied semianalytically in Ref. [39], (ii) a seed magnetic field with only $\tilde{A}^{i}(\tau_0) \neq 0$, which was covered before in the real-time lattice calculations of Ref. [40], and (iii) only $\tilde{j}^{i}(\tau_0) \neq 0$. (In the present linear-response analysis, the most general case is given by a linear superposition of these possibilities.)

A nonvanishing initial current $\tilde{j}^{i}_0(\tau_0)$ is provided by any nonzero function $\tilde{W}^0_i(k = 0, \nu; \phi, y - \eta_0)$ that is even in its last two arguments. In the following we simply take a constant

$$\tilde{W}^{\,0}_{i}(k = 0, \nu; \phi, y - \eta_0) = C_2, \tag{4.11}$$

which we found to be also representative of some more complicated possibilities that we have studied. Proceeding as above, this determines the function $\tilde{j}^{i}_0(\tau)$ in Eqs. (3.19) and (3.21) with C_2 proportional to the initial values $\tilde{j}^{i}(\tau_0)$.

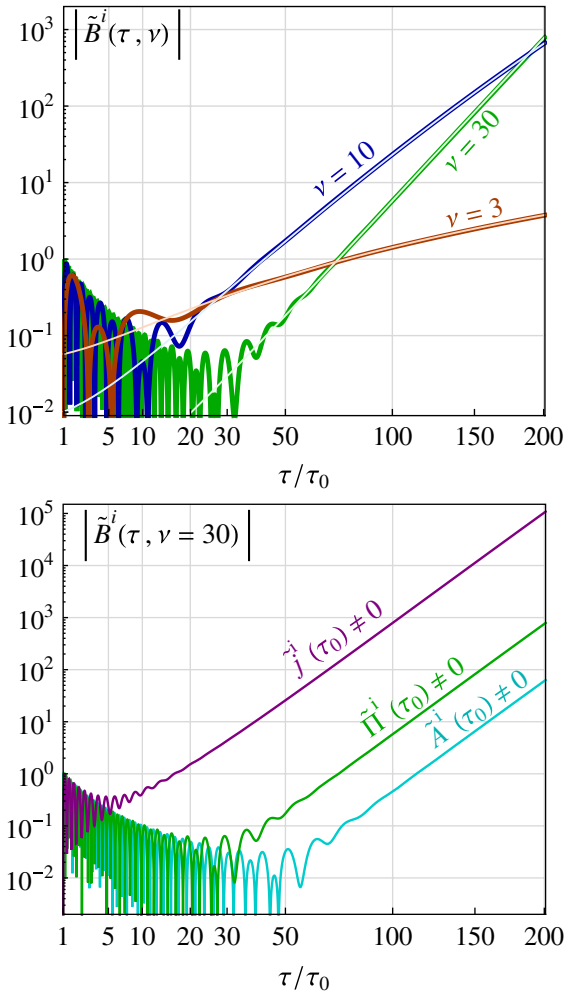

FIG. 2 (color online). Magnetic (Weibel) instabilities with $k = 0$ for an oblate momentum distribution from the beginning with $\tau_{\rm iso}/\tau_0 = 0.1$. In the upper panel transverse magnetic fields are compared for different wave numbers ν but equal initial conditions $\tilde{\Pi}^i(\tau_0) = 1$ and $\tilde{A}^i(\tau_0) = \tilde{j}^i(\tau_0) = 0$. The expected analytical late-time behavior, Eq. (A11), is indicated by the thin light lines. In the lower plot the influence of different initial values is studied for modes with $\nu = 30$.

In the upper part of Fig. 2 we consider the case (i) of an initial seed electric field for $\tau_{\rm iso}/\tau_0 = 0.1$ and compare with the analytic result for the late-time asymptotics (A11) for various values of ν. This is the analog to Fig. 1 of Ref. [39] but with our larger mass parameter[7] and less extreme initial anisotropy. Like Ref. [39] we observe a substantial delay in the onset of plasma instabilities which is preceded by a decay of collective fields until $\sim 10\tau_0$, suggesting an uncomfortable suppression of Weibel instabilities by the initial strong expansion of the plasma.

[7]As mentioned above, the recent CGC results [51] now favor this larger mass parameter, which was also considered in Ref. [39] but without corresponding plots.

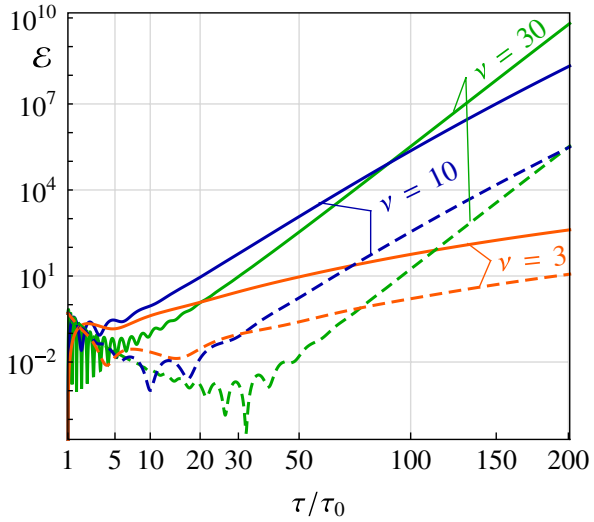

FIG. 3 (color online). Total energy density of Weibel instabilities for different wave numbers ν and $k = 0$, for $\tau_{\rm iso}/\tau_0 = 0.1$. The full lines correspond to $\tilde{j}^i(\tau_0;\nu) \neq 0$, while the dashed lines are the results for $\tilde{\Pi}^i(\tau_0;\nu) \neq 0$.

In the lower part of Fig. 2, the dependence of this behavior on initial conditions is displayed for mode $\nu = 30$. Case (ii) corresponds to using seed magnetic fields instead of seed electric fields, but this only increases the delay of plasma instabilities, which is in line with the results of [40] where mixed initial conditions for the fields were considered. Surprisingly enough, with case (iii) which corresponds to initial fluctuations in the currents, we find that this delay is very strongly reduced.

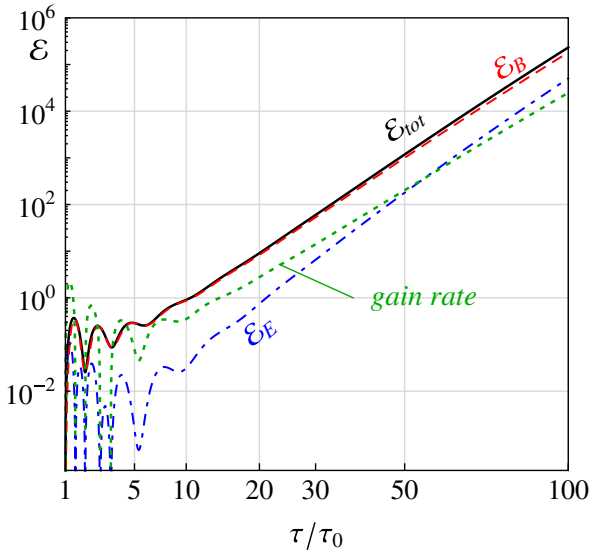

FIG. 4 (color online). The total energy density $\mathcal{E}_{\rm tot}$ for the mode with $\nu = 10$ and $\tilde{j}^i(\tau_0;\nu) \neq 0$ of Fig. 3 and its contributions from electric ($\mathcal{E}_E$) and magnetic fields ($\mathcal{E}_B$). Additionally the gain rate (times τ_0) is shown.

In Fig. 3 the comparison between cases (i) and (iii) is repeated for various values of ν, showing now the total energy in the collective fields, which confirms the finding of a drastic acceleration of the onset of plasma instabilities when there are initial current fluctuations. In Fig. 4 the energy density of one of those quickly growing modes ($\nu = 10$) is decomposed into magnetic and electric contributions together with the gain rate defined in Eq. (2.29).

From Fig. 3 one can also easily see the effect of having initial fluctuations in both induced currents and (chromo) electromagnetic fields. Because everything is linear, the resulting solutions are just linear combinations, and because the onset of exponential growth is so much quicker for the part corresponding to initial current fluctuations, such superpositions are dominated overwhelmingly by the latter as long as the two components have comparable initial energy densities. Since in the physical context of heavy-ion collisions we expect to find fluctuations in all quantities, induced currents (W fields) as well as gauge fields, we thus consider case (iii) as being actually representative of generic situations.

The strong reduction of the delay of the onset of Weibel instabilities makes it appear much more likely that plasma instabilities could play an important role in the very early dynamics of a quark-gluon plasma, at least with LHC energies, where $Q_s \sim 3$ GeV. Choosing $\tau_0 \sim Q_s^{-1} \sim \frac{1}{15}$ fm/c and judging from the time it takes that the initial depletion of energy in the fastest mode is reversed in Fig. 3, one may set the scale where plasma instabilities kick in to $\sim$0.5 fm/c, whereas the less generic initial conditions with only seed fields and no currents considered previously in Refs. [39,40] would have given $\sim$3 fm/c. (RHIC energies would give values 2–3 times higher.)

B. Wave vector perpendicular to anisotropy direction

Another comparatively simple case is provided by a wave vector which is strictly perpendicular to the anisotropy direction, i.e. $\nu = 0$ and $k \neq 0$. In this case the integrodifferential equations for $\tilde{A}^1$, $\tilde{A}^2$, and $\tilde{A}_\eta$ again decouple, but the equations for $\tilde{A}^1$ and $\tilde{A}^2$ are no longer identical, so that we have three different modes. Now there are two stable modes: the purely electrical mode with polarization along the wave vector, described by $\tilde{A}^1$, and the ("α") mode $\tilde{A}^2$, where the electric field is transverse to both the wave vector and the anisotropy direction and the magnetic field pointing in the anisotropy direction. The third mode, $\tilde{A}_\eta$, where the electric field points in the anisotropy direction while the magnetic field is transverse to both the wave vector and the anisotropy direction, is stable for oblate anisotropies, but contains a magnetic Weibel instability for the prolate case. We shall therefore now consider $\tau_{\rm iso} > \tau_0$ so that we have an initial period of prolate anisotropy before the expansion changes that into an oblate one, where none of the $\nu = 0$ modes is unstable.

1. Stable modes

The purely electrical mode $\tilde{A}^1$ with polarization along the wave vector again requires initial W fields in order to satisfy the Gauss law constraint. One of the simplest choices is

$$\tilde{W}^0_1(k, \nu = 0; \phi, y - \eta_0) = C_3 \cos\phi \tag{4.12}$$

with a constant C_3 that is proportional to the initial value $\tilde{\Pi}_1(\tau_0; k)$ appearing in the initial Gauss law constraint

$$\tau_0 \tilde{j}^\tau(\tau_0; k) = -ik\tilde{\Pi}_1(\tau_0; k). \tag{4.13}$$

Mode $\tilde{A}^2$, which is transverse to both wave vector and anisotropy direction, does not need initial W fields to satisfy the Gauss law constraint. Because we are more interested in the influence of different initial conditions on the evolution of plasma instabilities, we shall only consider the simplest case of $\tilde{\Pi}^2(\tau_0) \neq 0$.

In Fig. 5 we compare the numerical results for the electric fields corresponding to the two stable modes $\tilde{A}^1$ and $\tilde{A}^2$ for $k = 0.1\tau_0^{-1}$ and $\tau_{\rm iso}/\tau_0 = 100$, with a time range so that both prolate and oblate anisotropies are appearing. As expected, only stable oscillatory behavior is found. We observe that the purely electrical (plasmon) mode has a smaller frequency than the transverse stable mode, which is qualitatively similar to the familiar behavior in the isotropic case [52]. Perhaps more surprising is the rather strong attenuation during the first oscillations which is even stronger in the longitudinal plasmon mode.

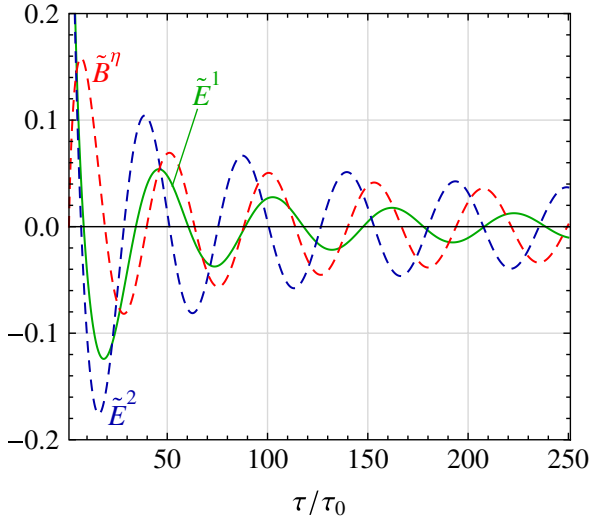

FIG. 5 (color online). Stable modes for wave vectors perpendicular to the anisotropy direction with $k = 0.1\tau_0^{-1}$, initial condition $\tilde{\Pi}_i(\tau_0; k) = 1$, and $\tau_{\rm iso}/\tau_0 = 100$. The full line corresponds to the longitudinal plasmon mode $\tilde{E}^1$, the dashed lines to electric and magnetic fields of transverse plasmons.

2. Weibel instability during prolate phase

In the time evolution of $\tilde{A}_\eta(\tau; k, \nu = 0)$, we expect to find magnetic Weibel instabilities for prolate anisotropies, thus only as long as $\tau < \tau_{\rm iso}$. In contrast to Weibel instabilities for oblate anisotropies there is now only one unstable mode, namely, with electric field transverse to the wave vector and pointing along the direction of anisotropy, and the magnetic field transverse to both.

We again consider initial conditions with and without initial currents. Nonzero initial induced currents $\tilde{j}^\eta$ can be set up most simply by choosing a constant $\tilde{W}^0_\eta(k, \nu = 0; \phi, y - \eta_0) = C_4$, which we compare with vanishing W^0_η and nonzero initial electric field, $\tilde{\Pi}^\eta(\tau_0) \neq 0$.

As before we choose $\tau_{\rm iso} \gg \tau_0$ to have an extended phase where the free-streaming plasma has prolate anisotropy, and we again stop the numerics only after the momentum distribution has become oblate.

Unfortunately, the numerical solutions show rather little activity with the mass parameter m_D extracted from CGC calculations. We therefore choose the much higher value $m_D^2 = 1000/(\tau_0\tau_{\rm iso})$ at first and consider the situation for our standard value only thereafter. Numerical results for the higher mass parameter and $\tau_{\rm iso} = 10\tau_0$ are displayed in Fig. 6(a), which exhibits a pronounced instability that shuts off when the degree of prolate anisotropy becomes too small for a given value of k. After that point in time, the mode decays for about as long as it was growing initially, ending in stable oscillations. Dashed lines correspond to nonzero initial values of $\tilde{\Pi}^\eta(\tau_0)$ and full lines to nonzero initial currents $\tilde{j}^\eta(\tau_0) \neq 0$, normalized such that the two different initial conditions have equal amplitude in the final oscillations. Since the solutions with nonzero initial currents reach larger maximal values we again find, although to a lesser degree, that such initial conditions are more efficient seeds for unstable modes.

In Fig. 6(b) the energy content in magnetic and electric fields is shown for one of the unstable modes, demonstrating that the energy is predominantly in magnetic fields, as expected for a Weibel instability. Near the point where the instability stops the electric field changes sign.

In Fig. 7 we finally consider our much smaller standard choice $m_D^2\tau_0\tau_{\rm iso} = 1.285$ and again the two initial conditions of nonzero initial electric field [upper plot, where $\tilde{\Pi}^\eta(\tau_0) = 1$] and nonzero initial current (lower plot), normalized so that the final oscillations have equal amplitude to first case. Also shown is the gain rate, defined in Eq. (2.29), times τ_0. Notice that the plot is now linear instead of logarithmic. In order to observe some instability, we need to consider much stronger initial anisotropy and $k \ll \tau_0^{-1}$. Figure 7 shows the various energy components for $\tau_{\rm iso} = 100\tau_0$ and $k = 0.1\tau_0^{-1}$.

Since the instability is now a magnetic one, its presence is best judged from the magnetic energy content. With initial electric seed field, the dominant effect is the transfer of the electric field energy to the hard particle background.

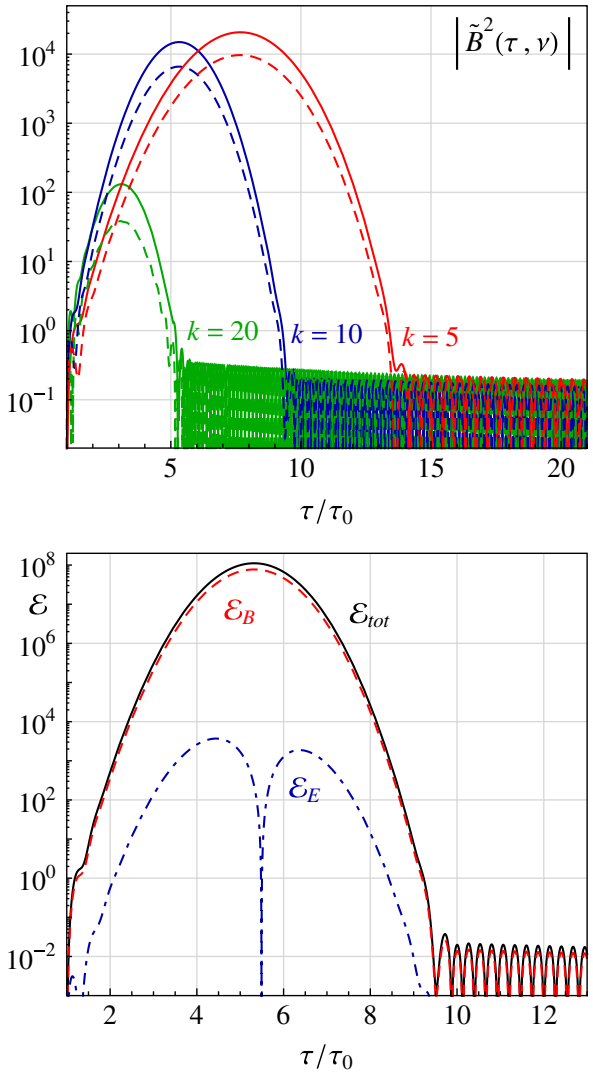

FIG. 6 (color online). Magnetic Weibel instabilities for initially prolate momentum distributions with $\tau_{\rm iso}/\tau_0 = 10$ for different wave numbers k (in units of τ_0^{-1}) and two different initial conditions (upper panel). The dashed lines correspond to $\tilde{\Pi}^\eta(\tau_0; k) \neq 0$ and the full lines to $\tilde{j}^\eta(\tau_0; k) \neq 0$. In the lower panel the total energy density and its contributions from electric and magnetic fields are shown for the mode with $k = 10\tau_0^{-1}$ and $\tilde{j}^\eta(\tau_0; k) \neq 0$. The mass parameter in both plots has been increased to $m_D^2 = 1000/(\tau_{\rm iso}\tau_0)$.

The magnetic field energy does increase, albeit nonmonotonically, without reaching the initial energy density supplied by the seed field. In the case of nonzero initial currents, there is a sharp initial increase in the energy density, which is however predominantly electric. The magnetic energy density eventually increases, too, again nonmonotonically, and only slightly higher than in the case with seed electric field.

We thus find that for our CGC-inspired mass parameter, the Weibel instabilities in the prolate phase (where the amount of prolate anisotropy decreases rapidly) are rather

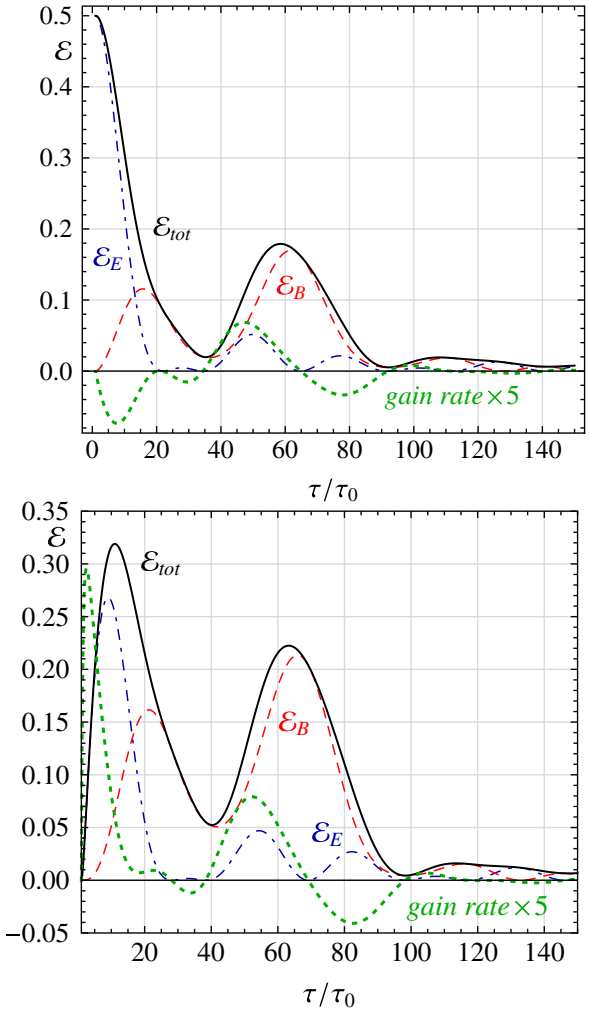

FIG. 7 (color online). Total energy densities and the contributions from electric and magnetic fields of prolate-phase Weibel instabilities with $k = 0.1\tau_0^{-1}$, $\tau_{\rm iso}/\tau_0 = 100$, and the CGC motivated Debye mass $m_D^2 = 1.285/(\tau_{\rm iso}\tau_0)$. The upper plot corresponds to the initial condition $\tilde{\Pi}^\eta(\tau_0) = 1$, the lower one to $\tilde{j}^\eta(\tau_0) \neq 0$. The gain rate (times τ_0, dotted line) is increased by a factor 5 to make it better visible.

weak when compared with the required energy densities in the initial seed configuration.

C. General wave vectors and electric instabilities

Up to now we have only considered the special situations where the integrodifferential equations for $\tilde{A}^1$ and $\tilde{A}^\eta$ were decoupled. We now turn to the more general case where this is no longer the case because both k and ν are nonzero. Such Fourier components correspond to a physical wave vector whose angle with the η (or z) axis increases with time according to $\vartheta = \arctan(\tau k/\nu)$.

In the oblate anisotropic case, the growth rate of unstable modes decreases with increasing ϑ. For the α mode the rate tends to zero as $\vartheta \to \pi/2$ and for the "$-$" mode already at $\leq \pi/4$. It is therefore of some interest to future 3 + 1-dimensional simulations of non-Abelian plasma instabilities to determine the range of wave numbers k for which the corresponding modes play an important part in the evolution.

Another interesting aspect of the generic case is that it allows us to study electric instabilities which appear in the "$-$" mode.

1. Electric instabilities for oblate anisotropy

When solving the coupled integrodifferential equations for $\tilde{A}^1$ and $\tilde{A}^\eta$ for nonzero k and ν we have again to take care of the nontrivial Gauss law constraint (3.24) at τ_0. To do so, we adopt the initial data for the W field of Eq. (4.1) also for nonzero k,

$$\tilde{W}^{\,0}_{\eta}(k, \nu; \phi, y - \eta_0) = C_5 \tanh(y - \eta_0), \tag{4.14}$$

where the constant C_5 is proportional to the initial electric field component parallel to the wave vector,

$$E_\parallel = \frac{k\tilde{\Pi}^1 + \nu\tilde{\Pi}^\eta}{\sqrt{k^2\tau^2 + \nu^2}}. \tag{4.15}$$

The electric field, lying in the 1-η plane, has in general also a component transverse to the wave vector, which we shall denote $E_\perp$ in this subsection. (The magnetic field is of course purely transverse and points in the 2-direction.)

An initial W field given by (4.14) gives rise to an initial charge density $\tilde{j}^\tau_0(\tau_0)$ as required by the Gauss law constraint, but zero initial spatial currents. In order to also have nonzero initial current components $\tilde{j}^\eta$ and $\tilde{j}^1$, we additionally add the components

$$\tilde{W}^{\,0}_{\eta,1}(k, \nu; \phi, y - \eta_0) = C_{6,7}. \tag{4.16}$$

As discussed in Sec. III C, we can expect to find an electric instability for wave vectors with nonvanishing $\vartheta < \pi/4$. Since ϑ increases with time, we choose small initial values of ϑ, which over some time satisfy the criterion of being within a 45° cone about the η axis.

In Fig. 8 the time evolution of the energy density for a mode with nonzero initial $\tilde{j}^1$ and $k\tau_0 = 1$, $\nu = 10$ is shown, for which we can expect an electric instability only for times smaller than $10\tau_0$. Again we consider a larger mass parameter $m_D^2 = 10/(\tau_{\rm iso}\tau_0)$ to find more significant results and indeed we notice that the total energy density rises initially with a significant electric component that is almost entirely longitudinal. After the maximum at about $4\tau_0$ we observe a strong decay and only small plasma oscillations after $10\tau_0$.

2. General magnetic instabilities for oblate anisotropy

For general wave vector and oblate anisotropy, the purely magnetic instabilities reside in the $\tilde{A}^2$ modes for all $\vartheta < \pi/2$, but with vanishing growth rates as $\vartheta \to \pi/2$. Nonvanishing initial currents can be simply taken into

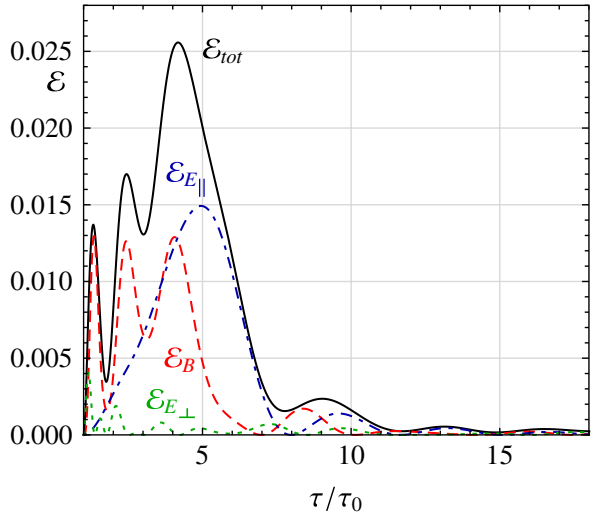

FIG. 8 (color online). Total energy density and the contributions from electric and magnetic fields for a mixed $\tilde{A}^{1,\eta}$ mode with $k\tau_0 = 1$ and $\nu = 10$ exhibiting an electric instability. The electric energy density is separated into a (dominant) longitudinal and a (small) transverse part with respect to the wave vector. The remaining parameters are $m_D^2 = 10/(\tau_{\rm iso}\tau_0)$ and $\tau_{\rm iso}/\tau_0 = 0.1$; the initial condition is $\tilde{j}^1(\tau_0; k, \nu) \neq 0$.

account by choosing a constant $\tilde{W}_2^0(k, \nu; \phi, y - \eta_0) = C_8$, with C_8 proportional to $\tilde{j}^2(\tau_0)$.

Using the same parameters as in Fig. 8, but now with nonzero initial $\tilde{j}^2$, we find an instability that is operative up to the somewhat larger time of about $6.5\tau_0$ (see Fig. 9) and which is almost completely in magnetic fields. For this set of parameters it was in fact crucial to have nonzero initial currents—with vanishing initial currents and only initial gauge fields we only found decreasing solutions.

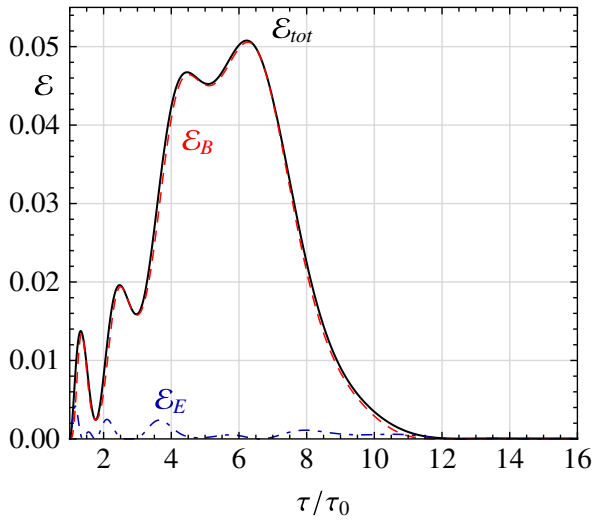

FIG. 9 (color online). Total energy density and its electric and magnetic contributions for the purely transverse $\tilde{A}^2$ mode with parameters as in Fig. 8 and initial condition $\tilde{j}^2(\tau_0; k, \nu) \neq 0$.

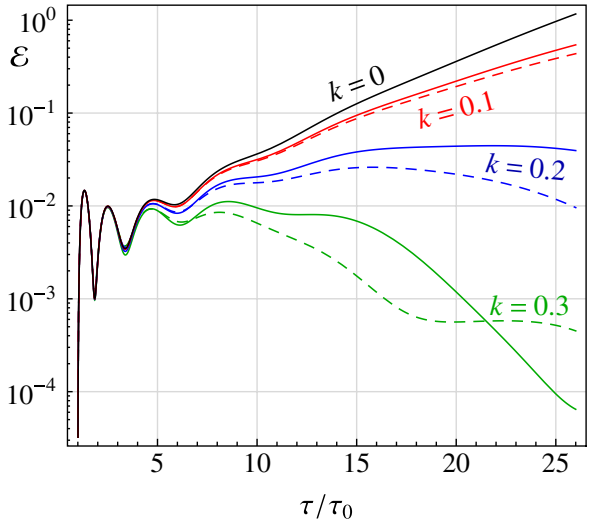

FIG. 10 (color online). Time evolution of unstable modes with $\nu = 10$ and various values of k (in units of τ_0^{-1}) and $\tau_{\rm iso}/\tau_0 = 0.1$. Full lines correspond to the purely transverse $\tilde{A}^2$ modes, dashed lines to the mixed $\tilde{A}^{1,\eta}$ modes, both with initial conditions of nonzero initial currents.

Returning to our standard choice of mass parameter, Fig. 10 displays the time evolution of the unstable modes with different values of k, the full lines corresponding to the $\tilde{A}^2$ modes, and the dashed ones to mixed $\tilde{A}^{1,\eta}$ ones. This shows that the most efficient plasma instabilities in the phase of oblate anisotropies are concentrated in the range $k \lesssim 0.2\tau_0^{-1}$.

V. SUMMARY AND CONCLUSIONS

In this paper we have generalized the semianalytical analysis of plasma instabilities in an anisotropically expanding plasma of Ref. [39] to general orientations of wave vectors and all possible polarizations of the individual Fourier modes. Moreover, we have generalized to arbitrary initial data in both the collective gauge fields and the W fields of the hard-loop formalism, which correspond to colored fluctuations in the hard particle distribution and thus directly to the induced currents.

Besides the well-studied magnetic (Weibel) instabilities of a plasma with oblate anisotropy, we have also considered plasma instabilities involving growing electric fields parallel to the wave vector. For the latter, the wave vector needs to have a nonzero angle with respect to the axis of expansion, which then increases with time, eventually shutting off such instabilities in the expanding case. We have also considered a plasma that starts with prolate anisotropy which after some time turns into an oblate one. Such instabilities have occasionally been conjectured to be the most interesting for isotropization in heavy-ion collisions [12]. However, we found that this type of Weibel instabilities requires plasma densities much larger than those suggested by CGC calculations.

For Weibel instabilities in the oblate phase, Ref. [39] has previously observed an uncomfortably long delay before they overcome the depletion of the energy in initial fields due to the (free-streaming) expansion of the plasma. With parameters taken over from CGC calculations, there seemed to be very little room for plasma instabilities for the available energies and plasma lifetimes at RHIC, while energies and plasma lifetimes expected for heavy-ion collisions at the LHC would make an important role conceivable, if the quark-gluon matter to be produced there turns out to be sufficiently weakly coupled to behave as a plasma.

However, Ref. [39] has considered only initial fluctuations in collective fields as seeds for plasma instabilities, while physically one should expect fluctuations in both collective fields and in the initial hard particle distribution. With our more general initial conditions that allow also for fluctuations in the initial hard particle distribution and the corresponding induced currents, we find much more favorable conditions for plasma instabilities. When the initial fluctuations in (only) induced currents are such that they give rise to the same energy content in collective modes as considered in the case of only initial field fluctuations, a surprisingly stark reduction of the delays of plasma instabilities by almost an order of magnitude was obtained. Because of linearity in the weak-field regime, this implies that the generic case of fluctuations of comparable strength in both induced currents and collective fields is overwhelmingly dominated by the modes corresponding to only initial current fluctuations.

In Sec. IV A 2 we have concluded that for LHC energies the time scales for plasma instabilities to set in are of the order of ~ 0.5 fm/c when initial current fluctuations are considered, while for RHIC energies these values would be about 2–3 times larger. Although for a significant backreaction of the plasma instabilities on the anisotropic hard particle distribution one would presumably have to consider times that are somewhat larger, this still seems to keep this mechanism very interesting at least for LHC energies.

Finally, we should emphasize that the present analysis was carried out in the weak-field (linear-response) regime. The nonlinear regime of quark-gluon plasma instabilities in the case of boost-invariant expansion was considered for an effectively 1 + 1-dimensional evolution in Ref. [40]. These results remain valid as far as the specific non-Abelian dynamics is concerned, but the uncomfortably long delay of the onset of the instabilities largely disappears by considering also initial fluctuations in the induced currents (equivalently, in the W fields). However, ultrarelativistic plasma instabilities have been found to behave very differently in the regime of a nonperturbatively large non-Abelian gauge field when a full 3 + 1-dimensional situation is considered. Work in this direction is in progress, for which the present semianalytical results will provide important cross-checks for the initial stages of the evolution of non-Abelian plasma instabilities.

ACKNOWLEDGMENTS

We thank Paul Romatschke and Mike Strickland for useful discussions, and Andreas Ipp for a careful reading of the manuscript. This work was supported by the Austrian science foundation FWF, Project No. P19526.

APPENDIX A: ANALYTICAL LATE-TIME BEHAVIOR

For modes with wave vector parallel to the anisotropy direction, i.e. $k = 0$ and $\nu \neq 0$, which is the case studied before in Ref. [39], the expressions for the induced currents simplify, and it is possible to study the late-time behavior of single modes analytically by expanding the contributions to the memory integrals around $\tau' = \tau$. Late-time behavior in our free-streaming approximation means extreme anisotropy, characterized by $\tau_{\rm iso}/\tau \equiv \theta \ll 1$. In this Appendix we recapitulate the analytical results of Ref. [39], filling in some details and also show that the late-time behavior is not modified by the necessity of including initial values for the longitudinal current in the case of longitudinal modes.

1. Transverse modes

With $k = 0$, the induced currents $\tilde{j}^i(\tau;\nu)$ are given by Eq. (4.9), where for simplicity we set $\tilde{A}^i(\tau_0;\nu) = 0$ and $\tilde{j}^i_0(\tau;\nu) = 0$. Expanding the integrand of the memory integral around $\tau' = \tau$ yields

$$\frac{i\nu\tau e^{i\nu\bar{\eta}'}\sinh\bar{y}}{\tau_{\rm iso}^2\sqrt{1+\frac{\tau^2\sinh^2\bar{y}}{\tau'^2}}} = \frac{i\nu\tau}{\tau_{\rm iso}^2}\left(\tanh\bar{y} + i\nu\tanh^2\bar{y}\left(1-\frac{\tau}{\tau'}\right) + \tanh^3\bar{y}\left(1-\frac{\tau}{\tau'}\right) + O\left[\left(1-\frac{\tau}{\tau'}\right)^2\right]\right). \tag{A1}$$

Terms odd in $\bar{y}$ give no contribution and neglecting the higher orders we obtain

$$\tilde{j}^i(\tau;\nu) \simeq -\frac{m_D^2}{4}\int\frac{d\bar{y}}{(1+\frac{\tau^2\sinh^2\bar{y}}{\tau_{\rm iso}^2})^2}\left\{\tilde{A}^i(\tau;\nu) + \int_{\tau_0}^{\tau}d\tau'\,\frac{\nu^2\tau\tanh^2\bar{y}}{\tau_{\rm iso}^2}\left(1-\frac{\tau}{\tau'}\right)\tilde{A}^i(\tau';\nu)\right\}. \tag{A2}$$

Using

$$\int \frac{d\bar{y}}{(1+\theta^{-2}\sinh^2\bar{y})^2} = \frac{(\theta^{-2}-2)\arctan(\sqrt{\theta^{-2}-1})}{(\theta^{-2}-1)^{3/2}} + \frac{1}{\theta^{-2}-1} = \frac{\pi\theta}{2} - \frac{\pi\theta^3}{4} + O(\theta^4) \tag{A3}$$

and

$$\int \frac{d\bar{y}\tanh^2\bar{y}}{(1+\theta^{-2}\sinh^2\bar{y})^2} = \frac{(2+\theta^{-2})\arctan(\sqrt{\theta^{-2}-1})}{(\theta^{-2}-1)^{5/2}} - \frac{3}{(\theta^{-2}-1)^2} = \frac{\pi\theta^3}{2} + O(\theta^4) \tag{A4}$$

for $\theta \equiv \tau_{\rm iso}/\tau \ll 1$, the transverse current reduces to

$$\tilde{j}^i(\tau;\nu) \simeq -\frac{\mu}{\tau}\tilde{A}^i(\tau;\nu) - \frac{\mu\nu^2}{\tau^2}\int_{\tau_0}^{\tau} d\tau' \tilde{A}^i(\tau';\nu)\left(1-\frac{\tau}{\tau'}\right), \tag{A5}$$

where $\mu = m_D^2\pi\tau_{\rm iso}/8$ and only terms up to linear order in $\tau_{\rm iso}/\tau$ have been kept. The equation of motion for the transverse gauge fields is

$$\left(\frac{1}{\tau}\partial_\tau\tau\partial_\tau + \frac{\nu^2}{\tau^2}\right)\tilde{A}^i(\tau;\nu) = \tilde{j}^i(\tau;\nu) \tag{A6}$$

and acting with $\partial_\tau^2\tau^2$ on it we eventually obtain an ordinary differential equation for each mode ν

$$\left(\partial_\tau^2\tau\partial_\tau\tau\partial_\tau + \nu^2\partial_\tau^2 + \mu\partial_\tau^2\tau - \frac{\mu\nu^2}{\tau}\right)\tilde{A}^i(\tau;\nu) \simeq 0. \tag{A7}$$

Simple results for the gauge fields are only obtained for very infrared modes $\nu \ll 1$, where all terms proportional to ν^2 can be neglected, or for high momentum modes $\nu \gg 1$, where only those terms proportional to ν^2 contribute. We find

$$\tilde{A}^i(\tau;\nu \ll 1) \simeq c_1 J_0(2\sqrt{\mu\tau}) + c_2 Y_0(2\sqrt{\mu\tau}), \tag{A8}$$

which is a stable oscillatory solution [$J_n(x)$ and $Y_n(x)$ are Bessel functions of the first and second kind, respectively], and

$$\tilde{A}^i(\tau;\nu \gg 1) \simeq c_1\sqrt{\tau}I_1(2\sqrt{\mu\tau}) + c_2\sqrt{\tau}K_1(2\sqrt{\mu\tau}), \tag{A9}$$

with $c_{1,2}$ being constants. The modified Bessel functions K_n and I_n have the asymptotic behavior $K_n(x) \simeq \exp(-x)/\sqrt{2\pi x}$ and $I_n(x) \simeq \exp(x)/\sqrt{2\pi x}$, where the latter describes a rapidly growing mode. Therefore we expect that large ν modes will be dominant at sufficiently late times with a behavior of

$$\tilde{A}^i(\tau) \sim \tau^{1/4}\exp(2\sqrt{\mu\tau}). \tag{A10}$$

For $\nu \sim 1$ the solutions can be written in terms of generalized hypergeometric functions ${}_2F_3$ and a Meijer G function [39]. The dominant contribution is

$$\tilde{A}^i(\tau;\nu)/\tau \sim {}_2F_3\left(\frac{3-\sqrt{1+4\nu^2}}{2}, \frac{3+\sqrt{1+4\nu^2}}{2}; 2, 2-i\nu, 2+i\nu, -\mu\tau\right), \tag{A11}$$

which is compared with the full semianalytical result in Fig. 2.

2. Longitudinal modes

For longitudinally polarized gauge fields we proceed analogously. In this case it is not *a priori* admissible to drop the term $\tilde{j}_0^\eta(\tau;\nu)$ in Eq. (3.20) because of the Gauss law constraint. However, numerically, we notice that at late times this contribution is negligible compared to the rest of the current, as can be seen in Fig. 11.

Omitting both $\tilde{j}_0^\eta(\tau;\nu)$ and the term proportional to $\tilde{A}_\eta(\tau_0;\nu)$, we can approximate Eq. (4.7) by

$$\tilde{j}^\eta(\tau;\nu) \simeq \frac{m_D^2}{2\tau_{\rm iso}^2}\int \frac{d\bar{y}\sinh^2\bar{y}}{(1+\frac{\tau^2\sinh^2\bar{y}}{\tau_{\rm iso}^2})^2}\left\{\tilde{A}_\eta(\tau;\nu) + i\nu\tanh^2\bar{y}\int_{\tau_0}^{\tau} d\tau'\tilde{A}_\eta(\tau';\nu)\frac{1}{\tau'^2}\left(1-\frac{\tau}{\tau'}\right)\right\}, \tag{A12}$$

where we have used again (A1), but with the factor $1/\tau_{\rm iso}^2$ replaced by $1/\tau'^2$. Using

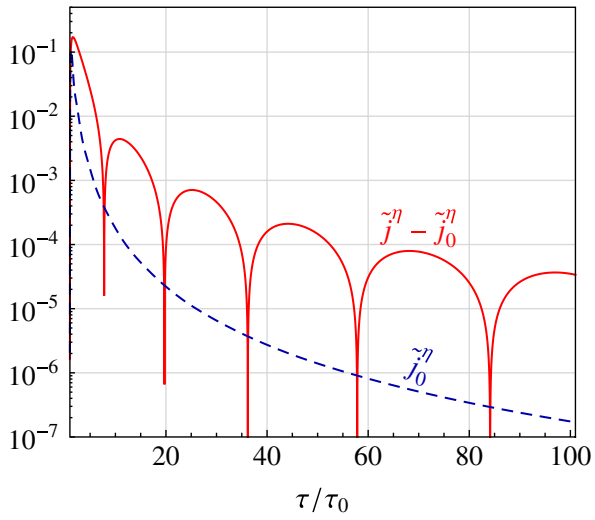

FIG. 11 (color online). The contribution from the current proportional to the initial conjugate momentum $\tilde{j}_0^\eta$ is negligible compared to the rest at late times. This data is for $\nu = 10$ and $\tau_{\rm iso}/\tau_0 = 0.01$.

$$\int \frac{d\bar{y}\sinh^2\bar{y}}{(1+\theta^{-2}\sinh^2\bar{y})^2} = \frac{\arctan(\sqrt{\theta^{-2}-1})}{(\theta^{-2}-1)^{3/2}} + \frac{1}{\theta^{-2}-\theta^{-4}} = \frac{\pi\theta^3}{2} + O(\theta^4) \tag{A13}$$

and

$$\int \frac{d\bar{y}\sinh^2\bar{y}\tanh^2\bar{y}}{(1+\theta^{-2}\sinh^2\bar{y})^2} = 2\theta^4 + O(\theta^5) \tag{A14}$$

for $\theta \equiv \tau_{\rm iso}/\tau \ll 1$, we obtain

$$\tilde{j}^\eta(\tau;\nu) \simeq \frac{2\mu}{\tau^3}\tilde{A}_\eta(\tau;\nu) + \frac{8\mu\nu^2\tau_{\rm iso}}{\pi\tau^3} \times \int_{\tau_0}^{\tau} d\tau' \tilde{A}_\eta(\tau';\nu)\frac{1}{\tau'^2}\left(1-\frac{\tau}{\tau'}\right). \tag{A15}$$

By acting with $\partial_\tau^2\tau^2$ on this expression we find

$$\partial_\tau^2(\tau^2\tilde{j}^\eta(\tau;\nu)) \simeq 2\mu\partial_\tau^2\left(\frac{\tilde{A}_\eta(\tau;\nu)}{\tau}\right) - \frac{8\mu\nu^2\tau_{\rm iso}}{\pi\tau^4}\tilde{A}_\eta(\tau;\nu), \tag{A16}$$

where we can neglect the second part for very large τ. The equation of motion for the longitudinal gauge fields therefore becomes

$$\left(\partial_\tau\frac{1}{\tau}\partial_\tau + \frac{2\mu}{\tau^2}\right)\tilde{A}_\eta(\tau;\nu) \simeq 0 \tag{A17}$$

and the late-time behavior is given by

$$\frac{\tilde{A}_\eta(\tau;\nu)}{\tau} \simeq c_1 J_2(2\sqrt{2\mu\tau}) + c_2 Y_2(2\sqrt{2\mu\tau}). \tag{A18}$$

This corresponds to stable and oscillatory solutions.

[1] D. Teaney, Phys. Rev. C **68**, 034913 (2003).
[2] P. Romatschke and U. Romatschke, Phys. Rev. Lett. **99**, 172301 (2007).
[3] H. Song and U. W. Heinz, Phys. Rev. C **77**, 064901 (2008).
[4] S. M. H. Wong, Phys. Rev. C **54**, 2588 (1996).
[5] S. M. H. Wong, Phys. Rev. C **56**, 1075 (1997).
[6] R. Baier, A. H. Mueller, D. Schiff, and D. T. Son, Phys. Lett. B **502**, 51 (2001).
[7] E. Shuryak, Prog. Part. Nucl. Phys. **62**, 48 (2009).
[8] P. Arnold, J. Lenaghan, and G. D. Moore, J. High Energy Phys. 08 (2003) 002.
[9] S. Mrówczyński, Phys. Lett. B **214**, 587 (1988).
[10] Y. E. Pokrovsky and A. V. Selikhov, JETP Lett. **47**, 12 (1988).
[11] S. Mrówczyński, Phys. Lett. B **314**, 118 (1993).
[12] J. Randrup and S. Mrówczyński, Phys. Rev. C **68**, 034909 (2003).
[13] A. H. Mueller, A. I. Shoshi, and S. M. H. Wong, Phys. Lett. B **632**, 257 (2006).
[14] D. Bödeker, J. High Energy Phys. 10 (2005) 092.
[15] P. Arnold and G. D. Moore, Phys. Rev. D **73**, 025013 (2006).
[16] A. H. Mueller, A. I. Shoshi, and S. M. H. Wong, Nucl. Phys. **B760**, 145 (2007).
[17] P. Arnold and G. D. Moore, Phys. Rev. D **76**, 045009 (2007).
[18] M. Asakawa, S. A. Bass, and B. Müller, Phys. Rev. Lett. **96**, 252301 (2006).
[19] S. Mrówczyński, A. Rebhan, and M. Strickland, Phys. Rev. D **70**, 025004 (2004).
[20] J. C. Taylor and S. M. H. Wong, Nucl. Phys. **B346**, 115 (1990).
[21] E. Braaten and R. D. Pisarski, Phys. Rev. D **45**, R1827 (1992).
[22] J. Frenkel and J. C. Taylor, Nucl. Phys. **B374**, 156 (1992).
[23] V. P. Nair, Phys. Rev. D **50**, 4201 (1994).
[24] J.-P. Blaizot and E. Iancu, Nucl. Phys. **B417**, 608 (1994).
[25] J.-P. Blaizot and E. Iancu, Nucl. Phys. **B421**, 565 (1994).
[26] P. F. Kelly, Q. Liu, C. Lucchesi, and C. Manuel, Phys. Rev. D **50**, 4209 (1994).
[27] J.-P. Blaizot and E. Iancu, Phys. Rep. **359**, 355 (2002).
[28] P. Romatschke and M. Strickland, Phys. Rev. D **68**, 036004 (2003).
[29] P. Romatschke and M. Strickland, Phys. Rev. D **70**, 116006 (2004).
[30] B. Schenke, M. Strickland, C. Greiner, and M. H. Thoma, Phys. Rev. D **73**, 125004 (2006).
[31] B. Schenke and M. Strickland, Phys. Rev. D **74**, 065004 (2006).
[32] A. Rebhan, P. Romatschke, and M. Strickland, Phys. Rev. Lett. **94**, 102303 (2005).
[33] P. Arnold, G. D. Moore, and L. G. Yaffe, Phys. Rev. D **72**, 054003 (2005).
[34] A. Rebhan, P. Romatschke, and M. Strickland, J. High Energy Phys. 09 (2005) 041.
[35] P. Arnold and G. D. Moore, Phys. Rev. D **73**, 025006 (2006).
[36] J. Berges, S. Scheffler, and D. Sexty, Phys. Lett. B **681**, 362 (2009).
[37] A. Dumitru, Y. Nara, and M. Strickland, Phys. Rev. D **75**, 025016 (2007).
[38] D. Bödeker and K. Rummukainen, J. High Energy Phys. 07 (2007) 022.
[39] P. Romatschke and A. Rebhan, Phys. Rev. Lett. **97**, 252301 (2006).
[40] A. Rebhan, M. Strickland, and M. Attems, Phys. Rev. D **78**, 045023 (2008).
[41] E. Iancu and R. Venugopalan, in *Quark-gluon Plasma 3*, edited by R. C. Hwa and X.-N. Wang (World Scientific, Singapore, 2003), pp. 249–336.
[42] J. D. Bjorken, Phys. Rev. D **27**, 140 (1983).
[43] G. Baym, Phys. Lett. **138B**, 18 (1984).

[44] A. H. Mueller, Phys. Lett. B **475**, 220 (2000).
[45] E. S. Weibel, Phys. Rev. Lett. **2**, 83 (1959).
[46] L. D. McLerran and R. Venugopalan, Phys. Rev. D **49**, 2233 (1994).
[47] R. Baier, A. H. Mueller, D. Schiff, and D. T. Son, Phys. Lett. B **539**, 46 (2002).
[48] Y. V. Kovchegov, Nucl. Phys. **A692**, 557 (2001).
[49] A. Krasnitz and R. Venugopalan, Nucl. Phys. **A698**, 209 (2002).
[50] A. Krasnitz, Y. Nara, and R. Venugopalan, Nucl. Phys. **A727**, 427 (2003).
[51] T. Lappi, Eur. Phys. J. C **55**, 285 (2008).
[52] H. A. Weldon, Phys. Rev. D **26**, 1394 (1982).